Final Report:

Telecommunications and Earth Observations Applications for Polar Stationary Solar Sails

National Oceanic and Atmospheric Administration (NOAA)

to

University of Glasgow, Department of Aerospace Engineering

Report Author

Professor Colin R McInnes
Department of Aerospace Engineering
University of Glasgow
Glasgow G12 8QQ
Scotland, UK

colinmc@aero.gla.ac.uk

NOAA Study Manager

Ms Patricia Mulligan
NOAA/NESDIS
FB4 5200 Auth Road
Suitland MD 20746-4304
USA

Patricia.Mulligan@noaa.gov

24 January 2003

Release 1.2

Summary

This report documents a study performed from November 2001 to January 2002 by the University of Glasgow, Department of Aerospace Engineering for the National Oceanic and Atmospheric Administration (NOAA).

The study provides an analysis of the solar sails to enable polar stationary orbits for a range of Earth observation and telecommunications applications. In particular:

- Near real-time imaging of arctic and Antarctic weather
- A data relay for the NPOESS satellite system
- A continuous communications channel for Antarctic bases

There appear to be significant advantages for such a polar stationary platform for low resolution imaging and for Antarctic telecommunications. Both high data rate (NPOESS) and low date rate (Geostorms) from satellite- to-satellite relay are also feasible with appropriate satellite subsystem design.

Index

1. Polar Stationary Orbits for Solar Sails

1.1 Polar Stationary Orbit Concept

Solar sails utilise the flux of momentum transported by photons from the Sun as a source of motive force. As such, they provide an ideal form of propulsion for high-energy missions, and indeed can enable entirely new concepts for deep space missions (appendix A). While the early development of solar sailing centred on concepts for large sails, recent developments in payload miniaturisation have led to much more modest sail concepts. In addition, it has been realised only recently that solar sails offer the possibility of unique, non-Keplerian orbits with novel mission applications.

One particular family of non-Keplerian orbits is obtained in the Sun-Earth system where new artificial equilibrium points may be generated. These new equilibrium points are similar to the classical Lagrange gravitational balance points, but their location can be selected by an appropriate choice of solar sail mass per unit area and sail orientation. Of particular interest are equilibrium points displaced sunward of the L_1 Lagrange point or displaced above the L_1 point, high above the ecliptic plane on the day-side of the Earth. Locations sunward of L_1 provide an ideal location to provide early warning of solar storms, which is the concept for the NOAA/DoD Geostorm mission. Locations high above L_1 provide a vantage point above the ecliptic plane for whole Earth imaging of the polar regions or for high latitude communications. In addition, locations high above the night-side of the Earth (associated with equilibria sunward of the L_2 Lagrange point) are also possible, although the sail performance requirements are significantly more demanding than for day-side equilibria.

Previous studies of novel mission applications for these artificial equilibria by RL Foward have proposed various modes of operation using a range of orbits – “polesitters”. It is has been found though that when a realistic solar sail with non-perfect reflectivity is considered (appendix B), some of these modes of operation are not in fact possible. For example, it is found that it is not possible to have a solar sail permanently fixed above a pole of the Earth, as had been previously suspected. In addition, the volume of space within which equilibria are possible on the night-side of the Earth is severely constrained with a realistic sail.

In order to explore applications of the polar stationary orbit concept, an orbit will be considered such that the solar sail is displaced high enough above the ecliptic plane on the day-side of the Earth to be stationed directly over the north pole at the summer solstice, as shown in Fig. 1. From this vantage point a constant daylight view of the Arctic is available at the summer solstice. However, the equilibrium location is fixed relative to the Sun and the Earth. Therefore, six months later at the winter solstice, the solar sail is no longer directly over the north pole due to the fixed tilt of the Earth's polar axis as the Earth orbits the Sun. From this new vantage point a constant view of high latitude regions is still available though. A similar polar stationary orbit can be achieved for a solar sail stationed below the ecliptic plane above the Antarctic.

1.2 Solar Sail Requirements

Having briefly explored the geometry of polar stationary orbits, the solar sail performance requirements will now be investigated. It will be assumed that the sail is non-ideal and has a realistic reflectivity of 0.85. After some analysis (appendix B) the required solar sail mass per unit area and orientation required for equilibrium above the ecliptic plane can be obtained. It is found that for a given sail mass per unit area

there is a large surface attached to the L_1 point on which a solar sail will remain in equilibrium high above the day-side of the Earth, with the gravitational, light pressure and centripetal forces in balance. There is a somewhat more constrained surface extending from the L_2 point which allows equilibria high above the night-side of the Earth. However, as will be seen, these solutions near L_2 are not attractive for polar viewing applications due to their restricted viewing geometry. A section of the surfaces of sail mass per unit area is shown in Fig. 2. A boundary surface is also shown which defines limits to the volume of space within which equilibrium is possible.

To investigate the use of polar stationary orbits equilibria above both the day and night-side of the Earth will be considered. The day-side equilibria will be defined with two solar sails such that a sail is directly over the north pole at the summer solstice (sail_1_day) and a sail is directly over the south pole at the winter solstice (sail_2_day), as defined in Table. 1. It is found that for an orbit which positions the solar sail along the Earth's polar axis at the solstices, there is an optimum distance to station the solar sail from the Earth which will minimise the required sail performance. For the orbit geometry described above, this optimum distance is 3.9 million km (~610 Earth radii), with a required solar sail mass per unit area of 15.4 gm^{-2} (including payload). For comparison, current first generation solar sail concepts such as the NOAA/DoD Geostorm mission have a total solar sail mass per unit area of 29.5 gm^{-2} (including payload). A solar sail with a loading of less than 15.4 gm^{-2} will provide an equilibrium point stationed closer to the Earth. However, it should be noted that the closest possible polar distance is $2.5x10^6$ km, defined by the boundary surface shown in Fig. 2.

In addition to the day-side sails, two solar sails will also be considered on the night-side of the Earth, located on a surface attached to the L_2 point. Due to the constrained volume of space within which a realistic solar sail can be stationed on the night-side, the solar sails will have a smaller elevation above the ecliptic plane and will not be above the polar axis at any time during the year, as defined in Table. 1. As will be seen, the northern sail (sail_1_night) and southern sail (sail_1_night) still have reasonable coverage of the Arctic and Antarctic. The night-side solar sails are assumed to be located at a distance of $9x10^5$ km (~140 Earth radii) to provide equilibria closer to the Earth than the day-side solar sails, but without requiring unrealistically high sail performance. For this distance the required solar sail mass per unit area is 3.9 gm^{-2} (including payload), which is significantly more demanding than the performance required for the day-side solar sails.

Sail_id	**Polar Distance**	**Elevation (above/below ecliptic)**	**Sail Loading**
Sail_1_day	$3.9x10^6$ km	+66.5 deg	15.4 gm^{-2}
Sail_2_day	$3.9x10^6$ km	-66.5 deg	15.4 gm^{-2}
Sail_1_night	$9.0x10^5$ km	+45.0 deg	3.9 gm^{-2}
Sail_2_night	$9.0x10^5$ km	-45.0 deg	3.9 gm^{-2}

Table 1.1 Solar sail locations (sail reflectivity 0.85)

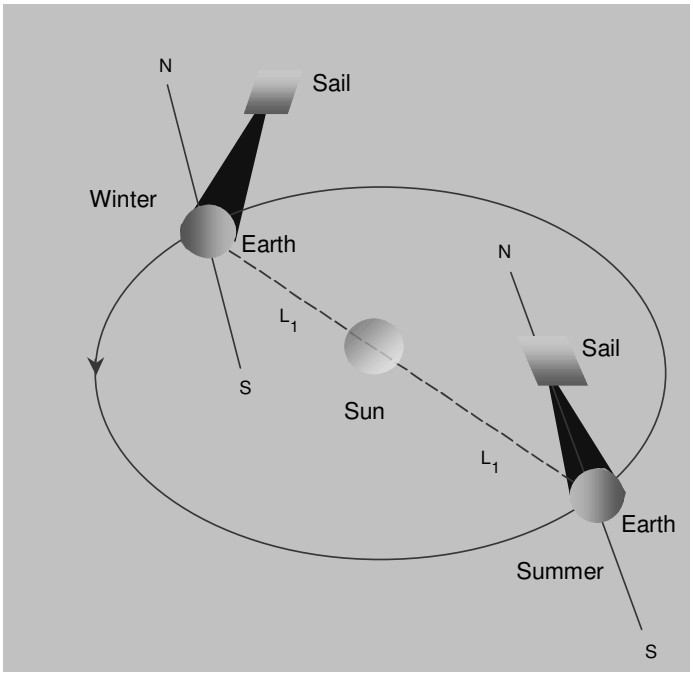

Figure 1.1 Schematic of Polar Observer concept for a day-side solar sail above the Arctic

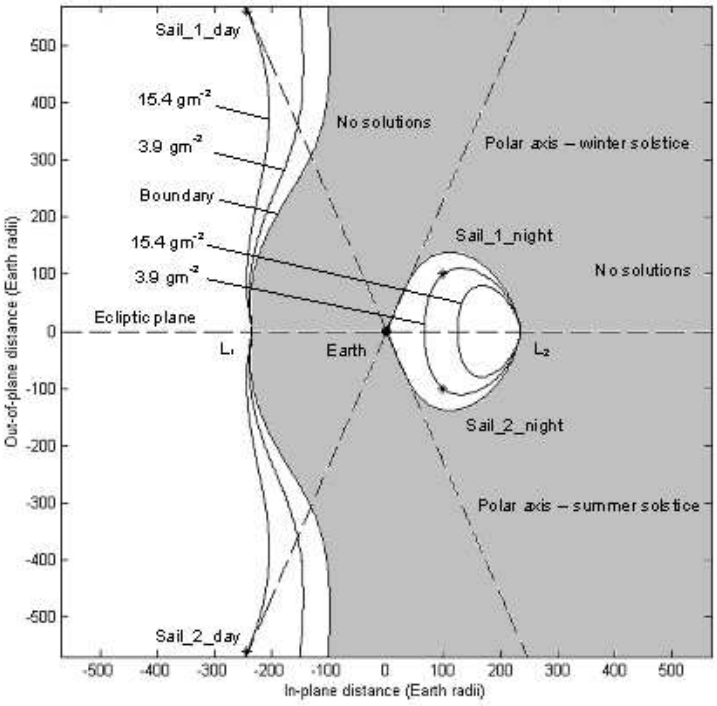

Figure 1.2 Solar sail locations on the day and night-side of the Earth above and below the ecliptic plane (*)

2. Earth Observation Applications

2.1 View from Day and Night Side Solar Sails

The polar stationary orbits have particular advantages and disadvantages. The distance of the solar sail from the Earth is larger than that used by conventional satellites for high resolution imaging. Sensor technology strategies which might mitigate this disadvantage will be discussed, and applications for more moderate imaging and remote sensing capabilities will be examined. One great advantage of the orbits is the ability to obtain real-time, continuous views of dynamic phenomena such as large scale polar weather systems which cannot be obtained from conventional polar orbiting satellites due to the lengthy period required to assemble a mosaic of images from individual polar passes. The utility of polar stationary orbits for such applications depends largely on the view obtained by the solar sails of high latitude polar regions.

The views obtained at the solstices and equinoxes for both northern and southern day-side solar sails are shown in Fig. 2.1 and 2.2. It can be seen that the northern solar sail is directly above the north pole at the summer solstice while the southern solar sail is directly above the south pole at the winter solstice, as discussed in section 1. Similar views are shown in Fig. 2.3 and 2.4 for the night-side solar sails. Since the elevation of the night-side solar sails above the ecliptic plane to lower than the day-side solar sails, the polar views are somewhat poorer with the north pole foreshortened at the summer solstice and the south pole foreshortened at the winter solstice.

2.2 Applications

For a 30 cm aperture instrument stationed 3.9 million km over the Arctic or Antarctic and operating at near optical wavelengths, a minimum ground resolution of order 10 km is possible, assuming ideal diffraction limited optics and neglecting the pointing stability of the camera. Higher resolution is possible if an equilibrium location closer to the pole is selected, at the expense of increased demands on the solar sail performance.

Instrumentation packages similar to those flown on GOES (e.g. multispectral imaging, etc.) could in principle be flown on a polar stationary platform, providing similar coverage over the poles, but at a degraded resolution.

Monitoring conditions over the polar regions as is done from the present generation of geosynchronous satellites could have significant implications for Antarctic research and operations. Such imaging capability would address a huge deficiency in current atmospheric science data collection capability. Furthermore, it could serve as a catalyst for the development of an Antarctic Meteorological Architecture which addresses many issues such as data collection, communications, processing/display, and archive in a coordinated manner. Indeed, should a polar stationary platform with an with atmopsheric sensor package be flown, it would likely be used in ways which cannot be currently imagined.

For imaging, at present multiple overpasses from NOAA polar-orbiters are assembled for retrievals of surface, cloud, and radiative properties over the Arctic andAntarctic (see http://stratus.ssec.wisc.edu/products/rtcaspr). However, it is not possible to obtain complete spatial coverage over a short time period with one satellite, and combining satellites introduces problems with geolocation and intercalibration. b

Therefore, a snapshot of the poles at regular time intervals, even at a spatial resolution of 10-25 km, is very desirable. Specific value is not limited to but includes: no data gaps, no missing data sectors, potential for much more frequent availability of imagery (near real-time).

If climate-related remote sensing over the Antarctic is indeed possible with a multi-spectral infrared sensor and with a spatial resolution of order 15-20 km applications for ice mass studies are also possible. With several infrared channels viewing without interruption the dynamical linkages between air masses over the southern ocean and water vapor/cloud advection may be observed, and hence moisture transport, over the high Antarctic plateau. This is related to the ice mass balance problem, which is currently the subject of a major new NASA satellite lidar mission (ICESAT).

Lastly, a useful imaging function may be provided by a night-side sail. For a 30 cm aperture instrument stationed at 900,000 km from the Earth and operating at infra-red wavelengths, a minimum ground resolution of order 40 km is possible, again assuming ideal diffraction limited optics and neglecting the pointing stability of the camera. Higher resolution is possible if an equilibrium closer location is selected, at the expense of increased demands on the solar sail performance.

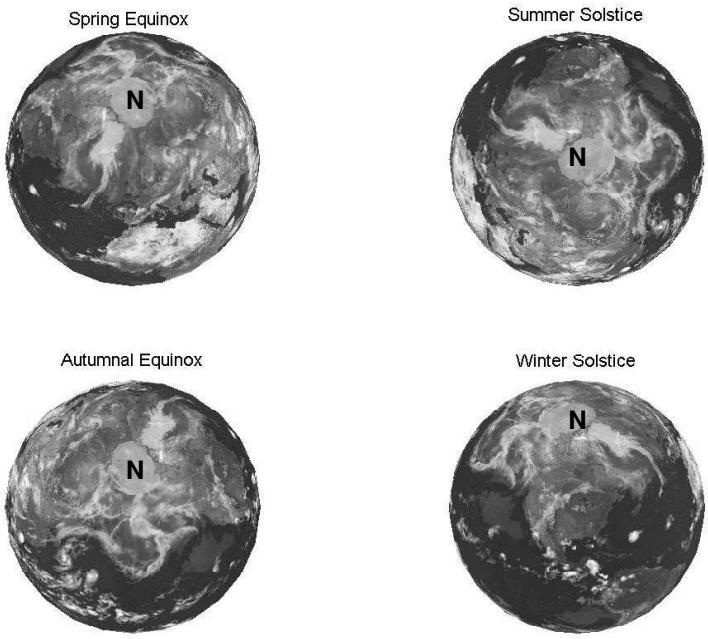

Figure 2.1 View from Sail_1 (North) on day-side

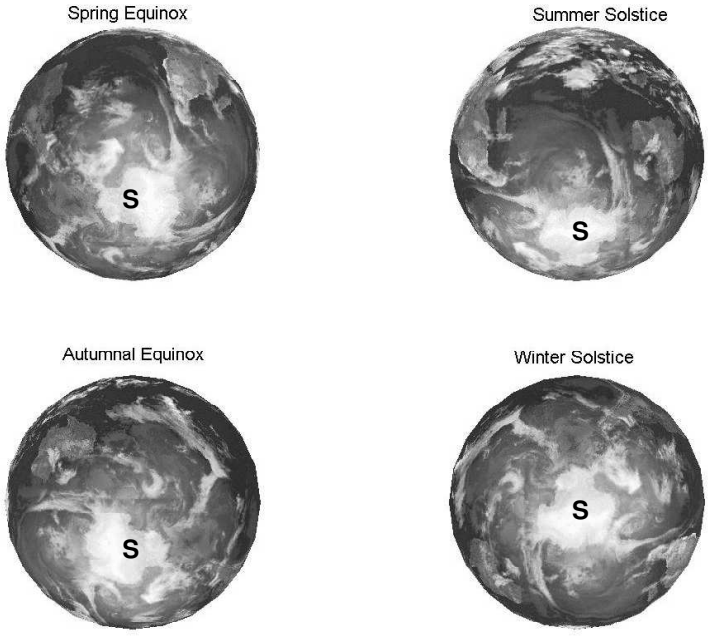

Figure 2.2 View from Sail_2 (South) on day-side

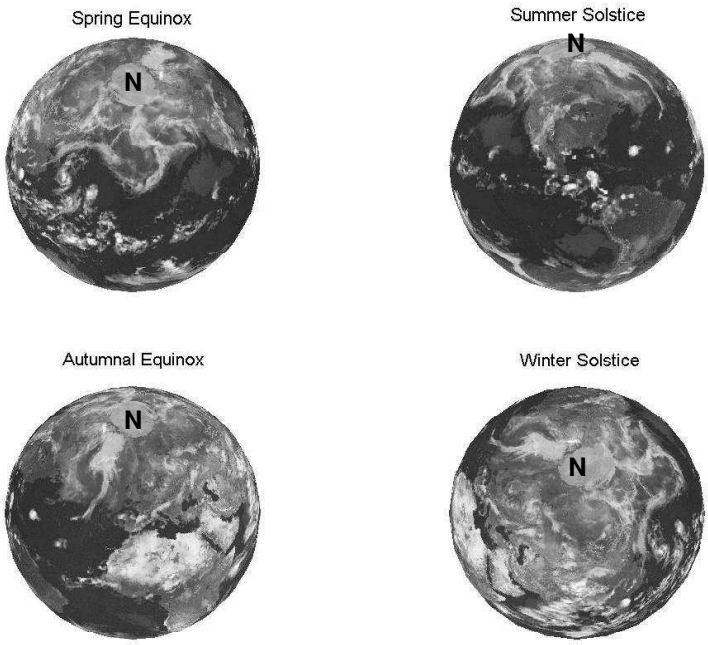

Figure 2.3 View from Sail_1 (North) on night-side

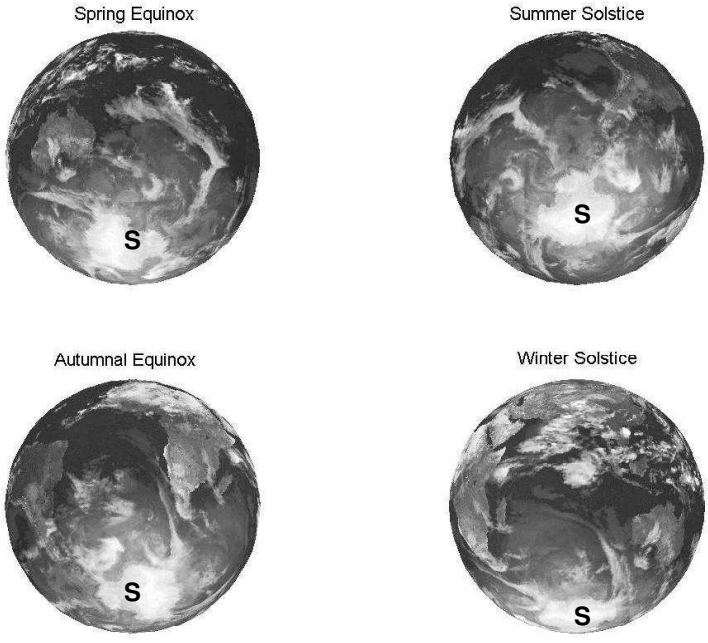

Figure 2.4 View from Sail_2 (South) on night-side

3. Telecommunications Applications

3.1 NPOESS Data Relay Concept

A major application of polar stationary orbits may the provision of data relay services for future NOAA polar orbiting satellites, such as the NPOESS system. In order to investigate the use of such orbits a model of the NPOESS system with two high latitude northern and southern CDAs (ground stations) and northern and southern solar sail polar relay platforms has been developed. The model determines the mutual visibility of a solar sail and member of the NPOESS system along with the elevation of each solar sail above the local horizon of its CDA. In this concept the solar sails would relay data from the NPOESS spacecraft through the high latitude CDAs to provide continuous coverage with only two relay spacecraft. However, the path length for data relay is long which necessitates the use of high equivalent isotropic radiated power (EIRP) for the down-link from the solar sails and/or a large antenna at the CDA facility to provide sufficient bandwidth for data returns from the NPOESS spacecraft. . . . .

The two CDAs which have been used for the investigation are the NOAA facilities at Point Barrow and McMurdo, as detailed in Table 3.1. The NPOESS system has been modelled as three spacecraft in Sun-synchronous near polar orbits with an azimuthal spacing of the orbit planes through the local time of the ascending node (LTAN), as detailed in Table 3.2. The visibility of the NPOESS spacecraft from both day and night-side solar sails will be investigated.

CDA_id	Name	Latitude	Longitude
CDA_1	Point Barrow	71.32 deg N	156.61 deg W
CDA_2	McMurdo	77.84 deg S	166.73 deg E

Table 3.1 CDA locations

Sat_id	Altitude	Inclination	LTAN
NPOESS_1	833 km	97.8 deg	13:30 hrs
NPOESS_2	833 km	97.8 deg	17:30 hrs
NPOESS_3	833 km	97.8 deg	21:30 hrs

Table 3.2 NPOESS orbits (local time of the ascending node LTAN)

3.2 Day-side Visibility

The visibility of each of the NPOESS satellites (NPOESS_1-3) from either day-side solar sail (sail_1 (north) or sail_2 (south)) will now be determined. It can be seen that NPOESS_1 and NPOESS_2 are always visible from either of the day-side solar sails providing a continuous path for data returns. NPOESS_2 (which is close to a dawn-dusk Sun-synchronous orbit) has short periods when the satellite is not visible from either day-side solar sail at the summer and winter solstices, as shown in Fig. 3.1. These coverage gaps are once per orbit, although the time step resolution of the model during the 1 year simulation does not capture this. Details of the coverage gaps will be explored later.

It can also be seen that the solar sails always appear well above the local horizon at the CDAs, as shown in Fig. 3.2. The elevation follows both a daily and an annual cycle with the amplitude of the daily cycle vanishing at the summer solstice for the northern CDA and the winter solstice for the southern CDA. At these times the solar sails are located along the polar axis and so have a fixed elevation relative to the local horizon.

In order to visualise the coverage of the NPOESS spacecraft, the visibility of each spacecraft from sail_1 (north) and sail_2 (south) is determined for a single orbit at the spring equinox, as shown in Fig. 3.3. It can be seen that there is an overlap in the visibility of each of the NPOESS spacecraft from each solar sail, providing continuous coverage. For example, the NPOESS_1 spacecraft is close to a noon-midnight Sun-synchronous orbit. Starting form the ascending equatorial crossing (at 13:30), sail_1 (north) can view the spacecraft for over half of the orbit until it falls behind the disk of the Earth. At this point sail_2 (south) can view the spacecraft, again allowing continuous coverage.

The coverage gaps of the NPOESS_2 spacecraft at the solstices can be seen in more detail in Fig. 3.4. Here, the visibility of the NPOESS spacecraft from sail_1 (north) and sail_2 (south) is shown for 2 orbits at the summer solstice. It can be seen that there is a short, once per orbit coverage gap for NPOESS_2 where it not visible from either sail_1 (north) or sail_2 (south). The gap appears at the descending equatorial crossing just before local dawn where the spacecraft has crossed the equator away from the two day-side solar sails. The coverage gap is however of relatively short duration (~2.5 minutes).

3.3 Night-side Visibility

The visibility of each of the NPOESS satellites (NPOESS_1-3) from either night-side solar sail (sail_1 (north) or sail_2 (south)) can also be determined. It can be seen that NPOESS_1 and NPOESS_2 have regular (once per orbit) coverage gaps for either of the night-side solar sails. NPOESS_2 (which again is close to a dawn-dusk Sun-synchronous orbit) has long periods when the satellite is in fact visible continuously from either night-side solar sail at the spring and autumn equinoxes, as shown in Fig. 3.5. The coverage gap for NPOESS_1 and NPOESS_2 is due to the lower elevation of the night-side solar sails above the ecliptic plane. When the spacecraft are close to their equatorial crossing on the day-side of the Earth they fall behind the disk of the Earth as viewed from the two night-side solar sails.

It can be seen that the elevation of the night-side solar sails above the local horizon at the CDAs can become extremely low. In particular, at the summer solstice sail_1 (north) appears close to the horizon as does sail_2 (south) and the winter solstice. Again, the solar sail elevation follows both a daily and an annual cycle.

Details of the regular coverage gaps which appear with the night-side solar sails can be seen in Fig. 3.7 and 3.8. Again, for NPOESS_1 starting form the ascending equatorial crossing (at 13:30), neither sail_1 or sail_2 can view the spacecraft until is moves part way around its orbit over the Arctic and is seen firstly by sail_1 (north) and then sometime later by sail_2 (south) as its orbits over the Antarctic. As the spacecraft moves along its orbit to the next equatorial crossing it is lost by sail_2 (south) and another coverage gap appears. Although the coverage gaps appear once per orbit, they are again of relatively short duration (~4.5 minutes).

3.4 NPOESS Data Relay Requirements

We considered a theoretical, and challenging case where a polesitter (here called NPRS) would relay a typical future meteorological/environmental polar orbiting satellite system's data to ground stations. The test case examined was the National Polar Orbiting Environmental Satellite System expected communications requirements. The expected advantage of such an architecture would be to lower the systems' data latency period to zero using two polesitters (with backup). The estimated cost of reducing data latency to zero using commercial geostationary assets is (provide number). The technical challenge of this case study is the difficulty of closing the EIRP over the long path length between the satellites.

The NPRS design trade space included four design cases performed by Edward Olsen, Aerospace Corporation (Edward.D.Olson@aero.org). The design trade-off included orbit locations of 900,000 km (night side) and 3,900,000 km (day side), and data rates of 20 Mbps and 40 Mbps. The trade study was performed calculating the EIRP required to close the link between the NPOESS and NPRS satellites. The study also examined different technical strategies to close the EIRP. These included increasing the NPRS aperature using two antennas (with attendant pointing considerations), using a 20 m antenna on NPRS, changing frequency to V band, coding changes, and using an optical communications design. Full details of the analysis are presented in Appendix C.

Additionally, technology readiness assessment of these suggested changes were performed by Robert Haw of NASA JPL (robert.haw@jpl.nasa.gov) and Steven Tyler (styler@ipac.caltech.edu) of the California Institute of Technology. Their analysis considers night side orbits at distances of 900,000 km and 625,000 km, with the lower altitude requiring a somewhat high performance solar sail. They concluded that cross-link communication between NPRS and NPOESS appears technically feasible with the current design, although some modest enhancements to the NPOESS baseline will be necessary (such as increasing transmitter power). But they also concluded that the current system design will not support the required downlink rate without significant and costly modification to the baseline NPRS architecture. Full details of the analysis are presented in Appendix D.

3.5 Antarctic Data Relay

The polar regions, particularly above 78^{o} of latitude, present significant challenges for high bandwidth, continuous communications. Since earth curvature prevents Geosynchronous Earth Orbiting (GEO) satellite visibility in the polar regions,, communications there must exploit multiple satellite constellations in contrast to the option of using only one GEO satellite at low latitudes. High Earth Orbit (HEO), also known as Molinya orbit, highly inclined Geosynchronous and Medium Earth Orbit (GEO and MEO) platforms are the most common satellite constellations suitable for high latitude locations. However, these approaches have limitations since they depend on satellite availability, unique ground station design, high costs, complexity, etc. when compared to the single GEO satellite system in use at lower latitudes.

For example, Amundsen-Scott South Pole Station has about 14.5 hours of high speed (greater than 256 kbps) off continent communications a day. MARISAT F2, GOES-3, and TDRSS F-1, all in GEO orbits inclined by about 12 degrees, provide this service through overlapping passes of between 5.5 and 6 hours a day. Figure 4.1 is shows the characteristic “figure 8” ground traces the satellites travel over during 24 hours of their orbit. The satellites are visible at South Pole when they are near the bottom of the “8”.

As an example of satellite visibility time at South Pole, Fig. 4.2 shows the elevation angle of GOES-3 as a function of time at South Pole. Note that it does not rise above 5 degrees. This is typical of platforms in this type of highly inclined GEO orbit. Unfortunately, low satellite elevation angles cause multi-path signal fades, particularly near the beginning and end of the pass due to signal reflections off the ice and tropospheric anomalous propagation effects which limit link efficiency. The elevation of an Antarctic polar stationary platform has been shown in Fig. 3.2.

A polar stationary satellite system could significantly improve polar communications, particularly in the southern hemisphere where Antarctic research activities and limited communications capabilities make a polar stationary platform very attractive. Possibilities include:

- 24 hour, 7 day a week high bandwidth (10 to perhaps 45 Mbps or more data rates) and 2-way inter- and intra-continental communication at fixed locations with large ground stations (eg. South Pole, McMurdo, Palmer, etc.)

- Continuous communication at rates up to 1.544 Mbps at sites with smaller antennas (eg. deep field camps, summer only research sites, vessels, etc.)

- Near real-time, continuously operating data links for scientific experiments and operational facilities at remote locations (e.g. automated weather stations, emergency airfields, etc.)

- Telemedicine activities and real-time monitoring and control of experiments

In addition to current polar telecommunications requirements there are plans to install a large neutrino experiment (~$200 million) at South Pole. Part of that project will address off-continent communications. A fibre optic cable is currently being considered to a satellite ground station at Dome Charlie (some 1000 km away) where geosynchronous satellites are visible. The likely cost of the fibre optic links is of order $80 million. If such an investment were to be directed to a multiuse polar stationary platform, a system which serves a much larger community both in terms of missions (e.g. atmospheric science, oceanography, glaciology, etc.) and geographically distributed communication users can be envisaged.

3.6 Geostorms Data Relay

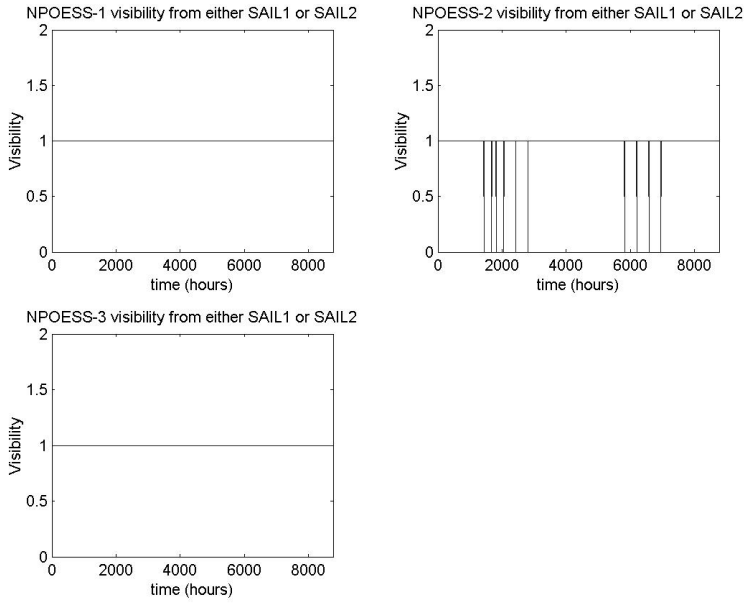

Figure 3.1 Visibility of the NPOESS spacecraft from either day-side solar sail (visible=1, not visible=0) – 1year from the Spring Equinox

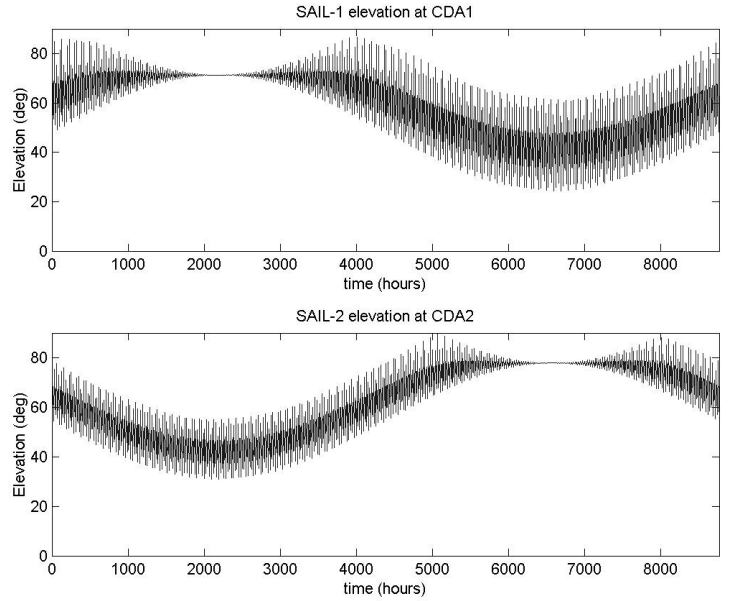

Figure 3.2 Day-side solar sail elevation above the CDA horizon – 1year from the Spring Equinox

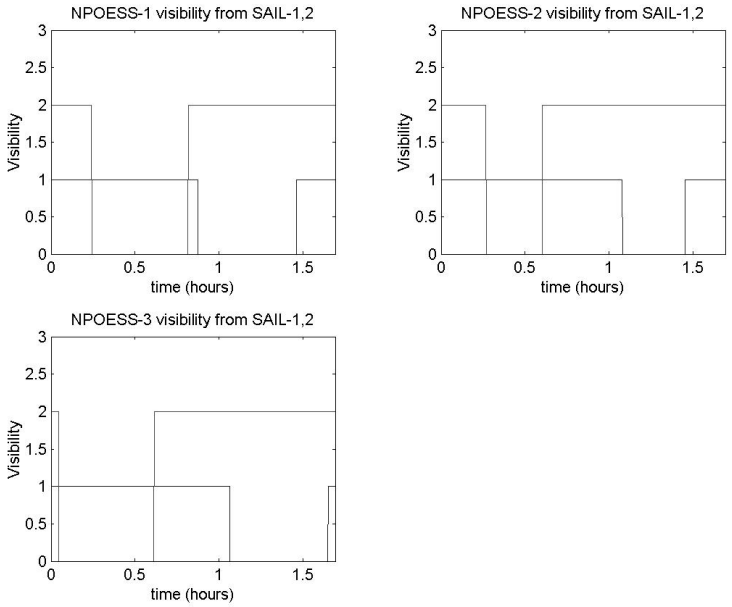

Figure 3.3 Visibility of the NPOESS spacecraft from the day-side sails (vis=1 for sail_1 and vis=2 for sail_2) – 1 orbit at the Spring Equinox

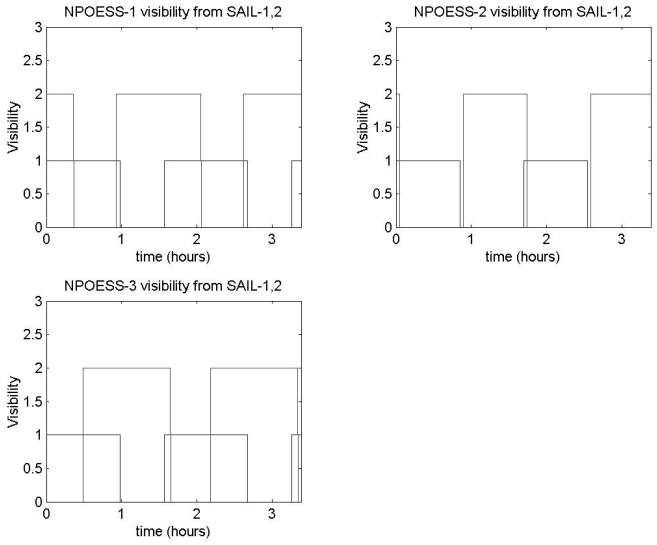

Figure 3.4 Visibility of the NPOESS spacecraft from the day-side sails (vis=1 for sail_1 and vis=2 for sail_2) – 2 orbits at the Summer Solstice

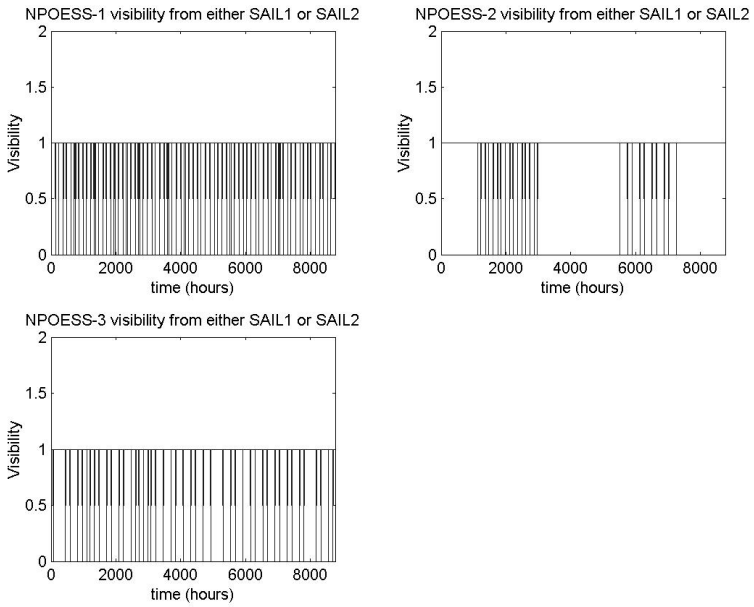

Figure 3.5 Visibility of the NPOESS spacecraft from either night-side solar sail (visible=1, not visible=0) – 1year from the Spring Equinox

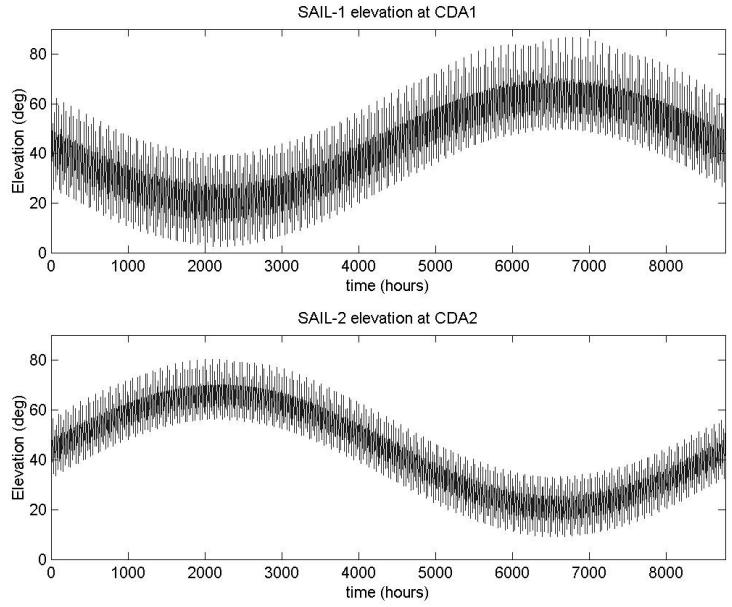

Figure 3.6 Night-side solar sail elevation above the CDA horizon – 1year from the Spring Equinox

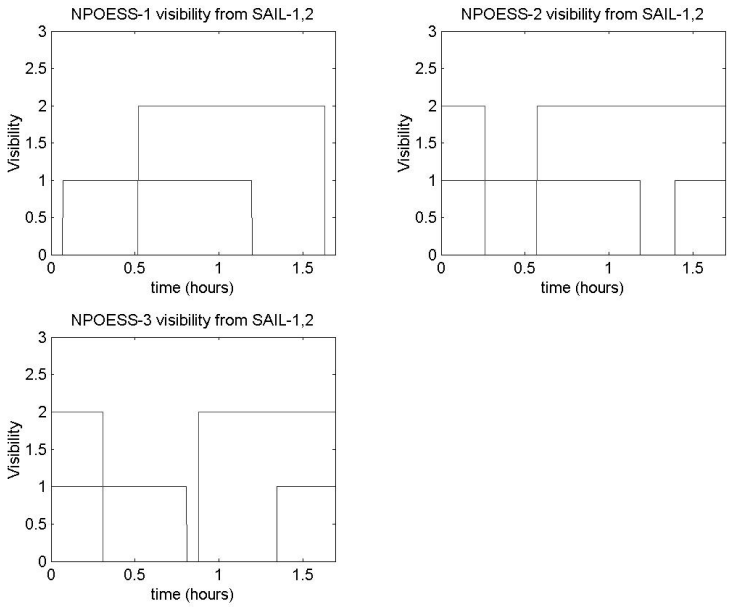

Figure 3.7 Visibility of the NPOESS spacecraft from the night-side sails (vis=1 for sail_1 and vis=2 for sail_2) – 1 orbit at the Spring Equinox

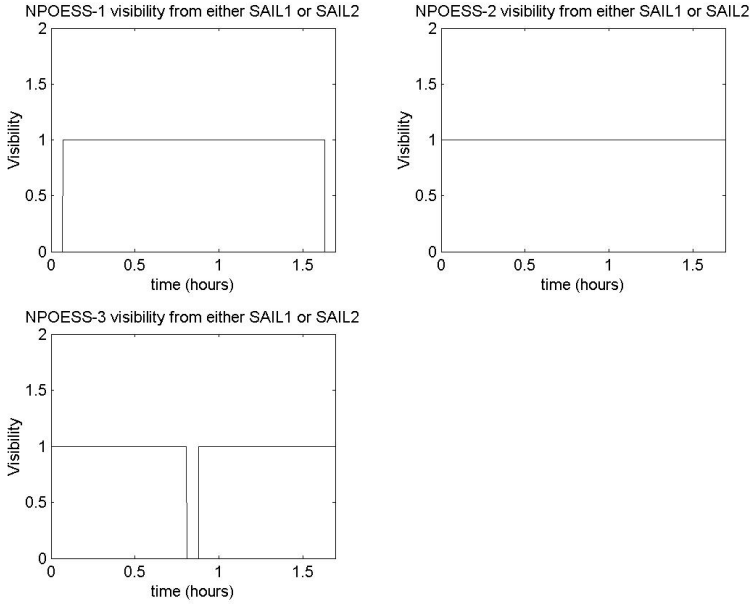

Figure 3.8 Visibility of the NPOESS spacecraft from either night-side sails (visible=1, not visible=0) – 1 orbit at the Spring Equinox

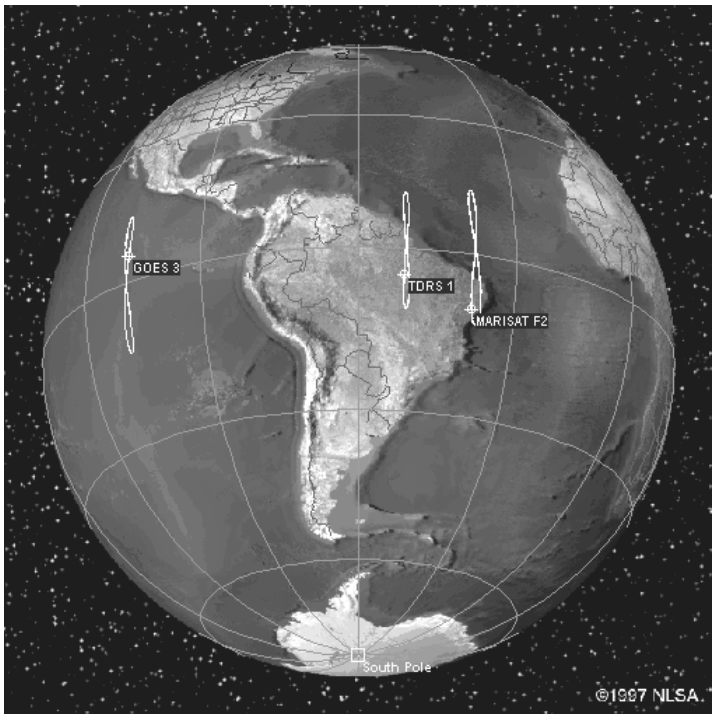

Figure 4.1 Ground tracks of GOES-3, TDFRS F1, and MARISAT F2

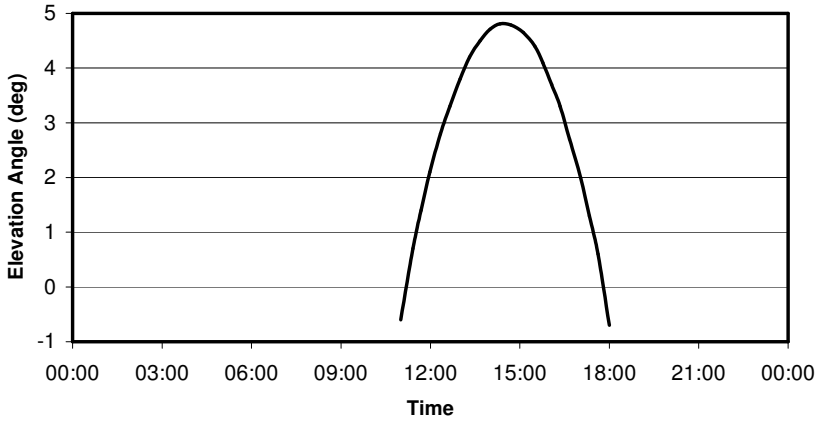

Figure 4.2 Typical GOES-3 elevation angle as a function of time as observed at Amundsen-Scott South Pole Station.

4. Conclusions

The use of polar stationary orbits has been investigated for solar sails stationed on both the day and night-side of the Earth. With modest technology improvements low data rate (~5Mbps) cross-link satellite applications are possible with polesitters in the near term, uses such as Geostorms data relay and NPOESS LRD downlink. Fuller use of the orbit for high data rate cross-link applications such as =>20Mbps will require more significant technology improvements which will be documented in a later phase of polesitter requirements now in process.

Acknowledgments

Section 2.2

Nicolas S. Powel, Raytheon Polar Services Company, 61 Inverness Dr East, Ste 300 Englewood CO 80112, 303 705-0714,powellni @polar.org

Jeffrey R. Key, NOAA/NESDIS, 1225 West Dayton St, Madison, WI 53706, 608 263-260, jkey@ssec.wisc.edu.

Matthew Lazzara, Antarctic Meteorological Research Center, Space Science and Engineering Center, University of Wisconsin-Madison 1225 West Dayton Street, Madison, WI 53706, 608 262-0436, mattl@ssec.wisc.edu

Dan Lubin, Associate Director, CalSpace/Scripps Institution of Oceanography, 9500 Gilman Drive, Dept. 0221, La Jolla, CA 92093-0221, 858 534-6369, dlubin@ucsd.edu

Section 3.4

Nicolas S. Powel, Raytheon Polar Services Company, 61 Inverness Dr East, Ste 300 Englewood CO 80112, 303 705-0714, powellni @polar.org

Robert J. Haw, NASA Jet Propulsion Laboratory, Oak Grove Drive, Pasadena, CA., robert.haw@jpl.nasa.gov.

Steven R. Tyler, California Institute of Technology, Pasadena, CA, styler@ipac.caltech.edu.

Appendix A. Introduction to Solar Sailing

A1. Concept

Solar sailing relies on solar radiation pressure, the flux of momentum transported by sunlight, to provide a useful propulsive force. Since solar sails do not require reaction mass they appear to offer the possibility of enabling new high energy mission concepts, and enhancing some existing mission concepts by significantly reducing launch mass. Future missions enabled by solar sails include a solar polar orbiter, multiple asteroid surveys and fast missions to the outer solar system. In addition, a range of so-called 'non-Keplerian orbits' have recently been defined which allow solar sails to be used to station payloads high over the poles of the Earth and maintain payloads continually within the geomagnetic tail. These missions do not use the solar sail solely as a payload transportation device, but as a means of providing unique viewpoints for innovative new science missions.

In order to extract momentum from incident sunlight, a solar sail requires a large tensioned metalised film to reflect photons. Combining the momentum of the incident photons with the reaction exerted by reflected photons, a propulsive force is generated normal to the sail surface. Therefore, by the rotating the sail this propulsive force can be directed and so orbit manoeuvring can be performed using suitable sail steering laws. Since the momentum transported by an individual photon is vanishingly small, solar sails clearly require a large surface area and a low total mass. The mass per unit area of the entire spacecraft for near term missions, the so-called sail loading, may be of order 30-15 gm^{-2}, generating an acceleration of order 0.25-0.50 mms^{-2}. An acceleration of 0.25 mms^{-2} is suitable for some deep space missions, while an acceleration of order 0.50 mms^{-2} is required for initial non-Keplerian orbit missions.

Achieving a useful acceleration from solar radiation pressure clearly poses engineering challenges in low mass deployable structures, thin films and payload miniaturisation. Existing thin films, such as DuPont Kapton, can be exploited for near term missions although thinner films provide benefits, particularly for large solar sails. Similarly, existing inflatable and deployable structures technologies can be used for near term missions, although large sails will require significant development

A.2 Configurations

Tensioning the solar sail can be achieved by applying forces at the edges of a large square sail film. These tension forces are induced by four booms whose stiffness properties must be sized to prevent buckling of the booms under compression. The spacecraft bus can then be attached in some manner at the central junction of the four booms (Fig. A1). This conventional design concept for a square solar sail requires deployable booms with high stiffness and a low specific mass, a means of folding, packing and extracting the sail film (possibly using the boom deployment process) and a method of attitude control. Attitude control can in principle be achieved by using small articulated reflectors at the boom tips to generate control torques or mounting the spacecraft bus on a gimballed mast normal to the sail film. By rotating the mast the centre-of-mass of the solar sail can be off-set from its centre-of-pressure, again inducing control torques.

An alternative design concept to the square solar sail is the so-called heliogyro. Here, the sail film is arranged in long, thin blades which are deployed from a rotating central hub which contains the spacecraft bus (Fig. A2). The blades of the heliogyro can be

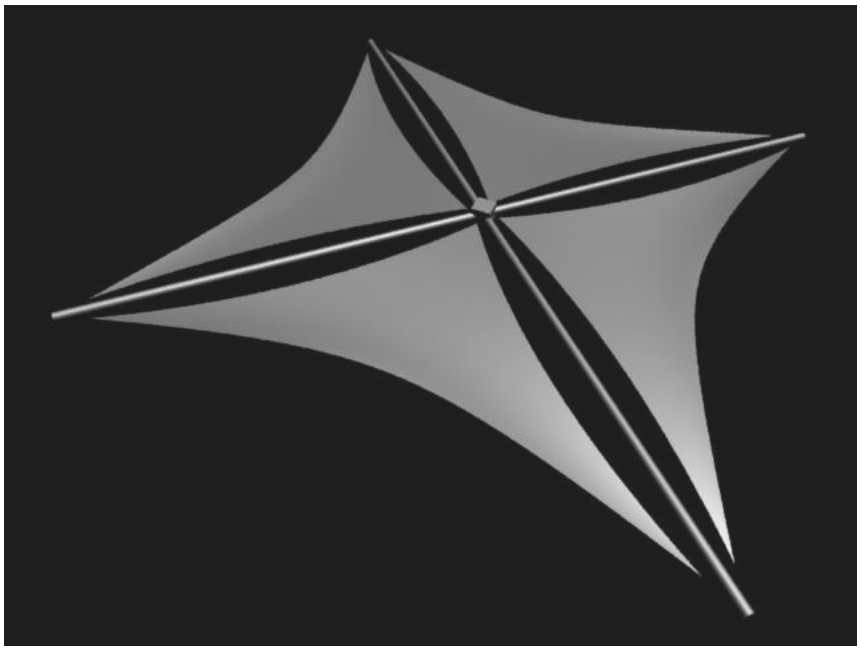

Figure A1 Square sail configuration

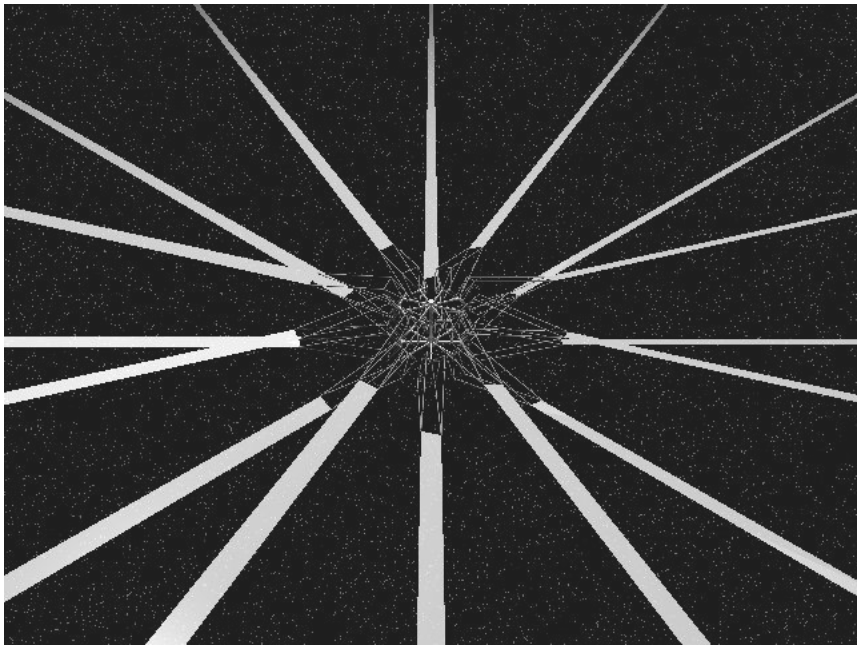

Figure A2 Heliogyro configuration

wound on rollers for launch, and then unwound under the action of spin induced tension for deployment. This is often seen as a more reliable deployment process than that used for the square solar sail. An additional perceived benefit of the heliogyro is that structural mass can be significantly reduced by using centripetal forces to tension the sail film, rather then compressive deployable booms. Attitude control is achieved by pitching the blades in a periodic manner to generate asymmetric forces across the blade disc, thus precessing the spin axis of the heliogyro. While deployment of the heliogyro appears simpler than the mechanical deployment of the square solar sail, issues arise associated with the control of large rotating structures, particularly with long slender blades.

A3. Agency Activities

NASA

In recent years NASA has sponsored the investigation of several new mission concepts for solar sails in considerable depth including a solar polar orbiter and a sub-L_1 solar storm warning mission. More far-term missions include the use of a high performance solar sail to reach the heliopause (100 AU) in less than 15 years. These advanced missions are in fact driving much of the early technology development work. In particular a novel, ultra-low mass carbon-fibre mat which can be metal coated has been developed by ESL Inc. for NASA/JPL. This metalised mat offers the possibility of high performance solar sails for a heliopause mission. Other materials activities have included the development of 1.5 μm CP1 polyimide film with integrated Kevlar ripstops by SRS Technologies for NASA. This film offers significant performance improvements over standard commercially available 7.5 μm Kapton film.

At the present time solar sailing is strongly established in NASA planning for future space science missions. This is reflected in the continuity of funding for mission studies and materials development and has recently been enhanced by the Gossamer Spacecraft Initiative and the $1B Living with a Star Initiative, both of which recognise solar sailing as a key technology. The Gossamer Spacecraft Initiative is funding novel concepts for large deployable structures with smart, multi-functional applications, such as the dual use of solar sails for propulsion and radio frequency antenna. A solar sail technology demonstration mission is in the critical path of the Gossamer Spacecraft Initiative technology roadmap and a NASA solar sail demonstration mission is under consideration for 2004-2005.

ESA

The main focus of European hardware development activities has been the DLR ODISEE demonstration mission study. This mission requires a 40 x 40 m sail to be launched to geostationary transfer orbit (GTO) on the Ariane V ASAP auxiliary payload ring, which imposes a launch mass limit of 120 kg. The primary goals of the mission are to demonstrate the fabrication, packing and deployment of a solar sail along with attitude control through centre-of-mass displacement. Recent ESA co-funded activities have centred on the ground test of a 20 x 20 m sail with carbon fibre reinforced plastic (CFRP) booms using 7.5 and 4 μm sail segments (Fig. A3, A4).

ESA has also funded mission studies at the University of Glasgow to assess the potential of solar sailing to enhance the long term space science goals of the agency. These studies have demonstrated that the existing COLOMBO Mercury orbiter mission could in principle be re-configured for a solar sail, leading to a reduction of the mission launch mass by up to 50%. Similarly, it was demonstrated that the existing SOLO solar physics mission could be re-configured for a solar sail, allowing a true solar polar orbit to be reached, rather than the more modest orbit inclined at only 40^{o} to the ecliptic which will be achieved with the base-line mission. Both COLOMBO and SOLO are base-lined for solar electric propulsion.

Figure A3 20 x 20 m sail deployment test 17 December – boom deployment

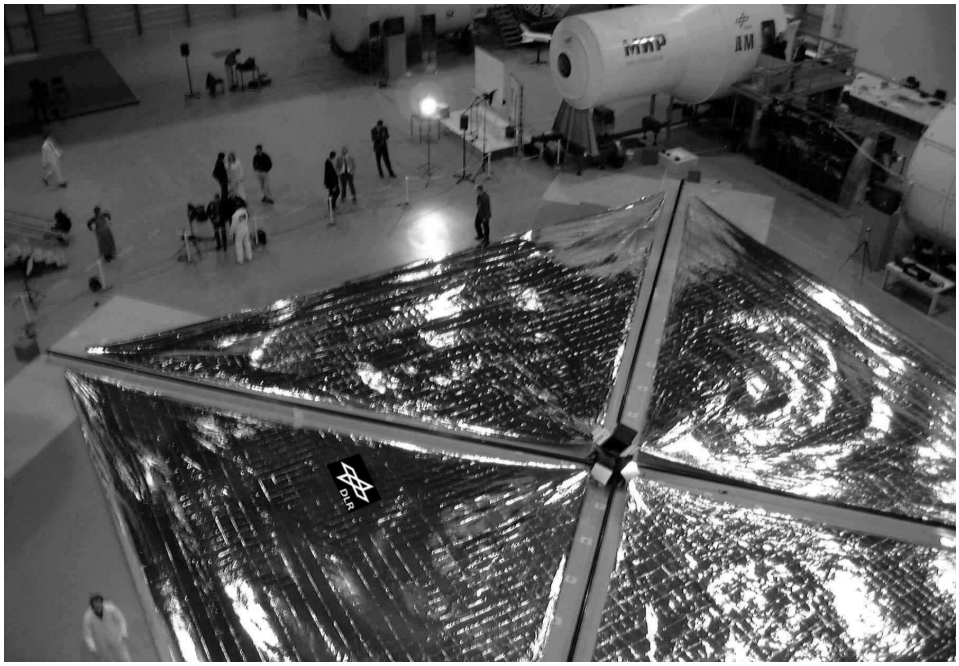

Figure A4 20 x 20 m sail deployment test 17 December 1999 – sail deployment

A4. Design Parameters

The fundamental measure of performance of a solar sail is its **characteristic acceleration**, defined as the solar radiation pressure acceleration experienced by the solar sail while oriented normal to the Sun-line at a heliocentric distance of 1 AU. The characteristic acceleration is a function of both the efficiency of the solar sail design and the mass of the payload. At a distance of 1 AU the magnitude of the solar radiation pressure P exerted on a perfectly absorbing surface is 4.56 x 10^{-6} Nm^{-2}. Therefore, allowing for the finite sail efficiency η of the sail, the characteristic acceleration a_o is defined by

$$a_o = \frac{2\eta P}{\sigma} \ , \ \sigma = \frac{m_T}{A} \qquad \text{(A.1)}$$

where σ is the **solar sail loading**, with m_T the total mass of the solar sail and A the sail area. The **sail efficiency** η is a function of both the optical properties of the sail film and the sail shape due to billowing and wrinkling. Eq. (A.1) can also be written as a useful sizing rule

$$a_o = \frac{9.12\eta}{\sigma\,[g\ m^{-2}]}\ [mms^{-2}] \qquad \text{(A.2)}$$

The total mass of the solar sail will now be partitioned into two components, the sail film and structural mass m_S and the payload mass m_P. Therefore, the characteristic acceleration of the solar sail may now be written as

$$a_o = \frac{2\eta P}{\sigma_S + (m_P / A)} \ , \ \sigma_S = \frac{m_S}{A} \qquad \text{(A.3)}$$

where σ_S is the mass per unit area of the sail assembly. This so-called **sail assembly loading** is a key technology parameter and is a measure of the thickness of the sail film and the efficiency of the solar sail structural and mechanical design.

Current European solar sail development work for a 40 x 40 m demonstration mission using CFRP booms, as discussed in section A3, projects a sail assembly loading of order 33 gm^{-2}. Other development work at NASA JPL to fabricate ultra-thin sail films could lead to a sail assembly loading of order 5 gm^{-2} or less for future missions.

A5. Solar Sail Sizing

Now that the key solar sail design parameters have been defined, the process of sizing a solar sail will be considered. From Eq. (A.3) it can be seen that the solar sail payload mass may be written as

$$m_p = \left[\frac{2\eta P}{a_o} - \sigma_s \right] A \qquad \text{(A.4)}$$

Similarly, from Eq. (A.1) the total mass of the solar sail may be written as

$$m_T = \frac{2\eta P A}{a_o} \qquad \text{(A.5)}$$

For a required characteristic acceleration, Eqs. (A.4) and (A.5) may now be used to size a solar sail while imposing constraints on the total mass of the solar sail to satisfy the capacity of the launch vehicle. Design charts are shown in Figs. A5 and A6 for

characteristic accelerations of 0.1-0.25 mms^{-2}, which are representative of technology demonstration missions. It is clear that for a small sail and high assembly loading only quite modest payloads can be transported. However, recent developments in payload miniaturisation and microsatellite technologies mean that such low mass payloads are still highly capable.

In addition to the design parameters discussed above, an additional parameter of interest can be defined. The **payload mass fraction** m_p/m_T of the solar sail can be obtained from Eqs. (A.4) and (A.5) as

$$\kappa = 1 - \frac{a_o \sigma_s}{2\eta P} \ , \ \kappa = \frac{m_P}{m_T} \qquad \text{(A.,6)}$$

This is clearly another key parameter and is a measure of the efficiency of use of the solar sail. The payload mass fraction for a range of characteristic accelerations is shown in Fig. A7. It is clear from Fig. A7 that advances in sail technologies to reduce the sail assembly loading can be used to two ways. Such improvements can increase the solar sail characteristic acceleration and so reduce trip times, or more importantly, for a fixed characteristic acceleration, can significantly increase the payload mass fraction of the solar sail. An improved payload mass fraction will lead to a more cost effective mission since a smaller launch vehicle may be used for the same payload mass. Alternatively, a larger science payload can be delivered by the solar sail for the same total launch mass.

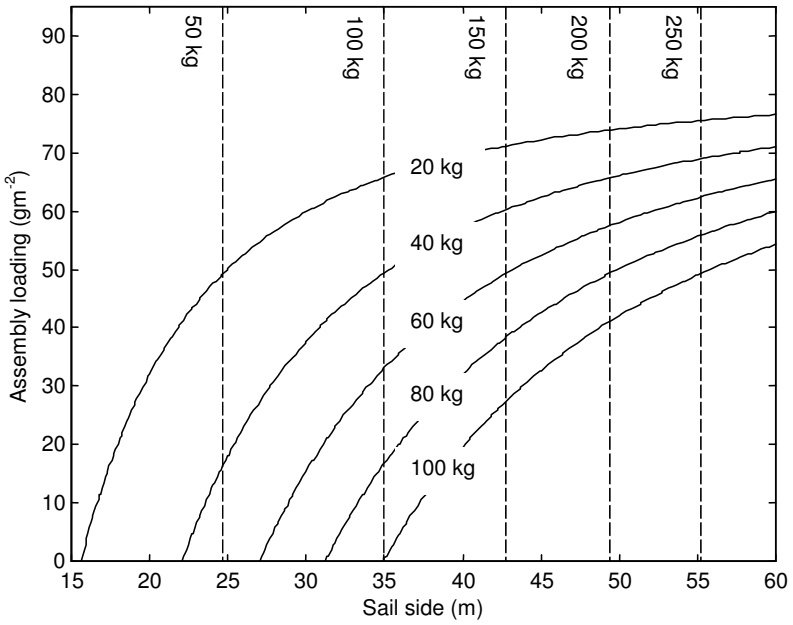

Figure A5 Design chart for a characteristic aceleration of 0.1 mms^{-2} and η=0.9 (solid line: payload mass, dashed line: total mass)

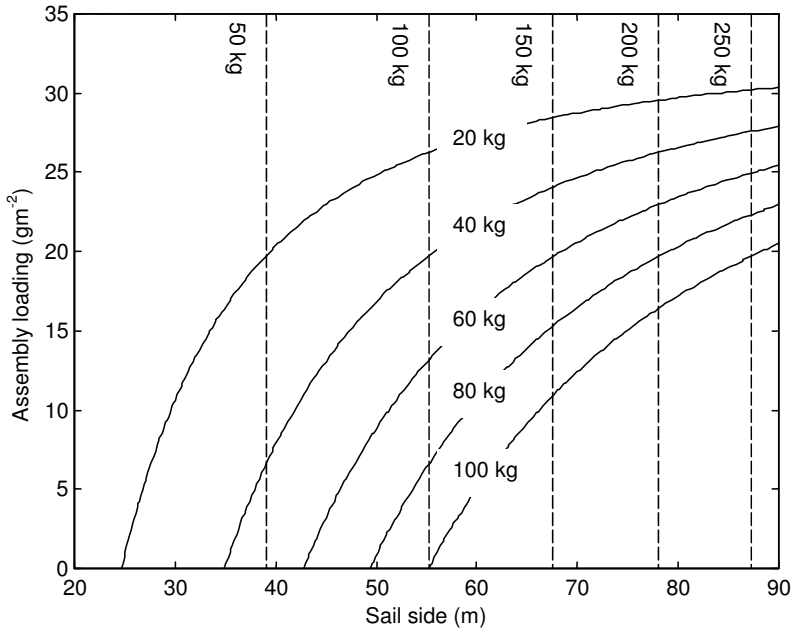

Figure A6 Design chart for a characteristic aceleration of 0.25 mms^{-2} and η=0.9 (solid line: payload mass, dashed line: total mass)

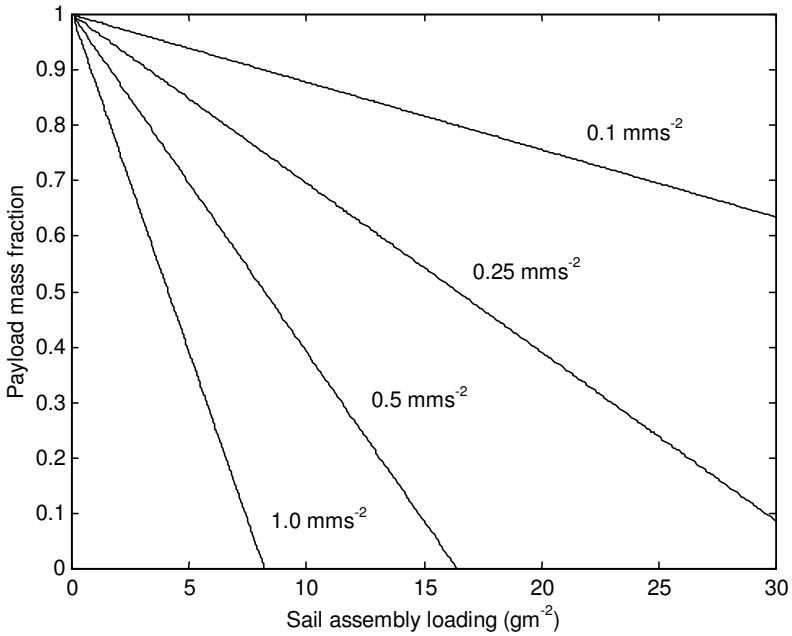

Figure A7 Solar sail payload mass fraction as a function of sail characteristic acceleration with η=0.9

A6. Further Reading

Introductory papers

Tsu, T.C., 'Interplanetary Travel by Solar Sail', American Rocket Society Journal, 29, 422-427, 1959

London, H.S., 'Some Exact Solutions of the Equations of Motion of a Solar Sail With a Constant Setting', American Rocket Society Journal, 30, 198-200, 1960

Sands, N., 'Escape from Planetary Gravitational Fields by use of Solar Sails', American Rocket Society Journal, 31, 527-531, 1961

Fimple, W.R., 'Generalised Three-Dimensional Trajectory Analysis of Planetary Escape by Solar Sail', American Rocket Society Journal, 32, 883-887, 1962

Wright, J.L. & Warmke, J.M., 'Solar Sail Mission Applications' AIAA-76-808, AIAA/AAS Astrodynamics Conference, San Diego, August 1976

Van der Ha, J.C. and Modi, V.J., 'Long-term Evaluation of Three-Dimensional Heliocentric Solar Sail Trajectories with Arbitrary Fixed Sail Setting', Celestial Mechanics, 19, 113-138, 1979

Forward, R.L., 'Light-levitated Geostationary Cylindrical Orbits', Journal of Astronautical Sciences, 29, 1, 73-80, 1981

Svitek, T. et. al., 'Solar Sail Concept Study', IAF-ST-82-12, 33rd International Astronautical Congress, Paris, October 1982

Staehle, R.L., 'An Expedition to Mars Employing Shuttle-Era Systems, Solar Sail and Aerocapture', Journal of the British Interplanetary Society, 35, 327-335, 1982

McInnes, C.R., 'Solar Sail Halo Trajectories: Dynamics and Applications', IAF-91-334, 42nd International Astronautical Congress, Montreal, October 1991

Forward, R.L., 'Statite: A Spacecraft That Does Not Orbit', Journal of Spacecraft and Rockets, 28, 5, 606-611, 1991

McInnes, C.R. McDonald, A.J.C. Simmons, J.F.L. & MacDonald, E.W., 'Solar Sail Parking in Restricted Three-Body Systems', Journal of Guidance Dynamics and Control, 17, 2, 399-406, 1994

Maccone, C., 'Space Missions Outside the Solar System to Exploit the Gravitational Lens of the Sun', Journal of the British Interplanetary Society, 47, 45-52, 1994

Leipold, M., Borg, E., Lingner, S., Pabsch, A., Sachs, R. & Seboldt, W., 'Mercury Orbiter with a Solar Sail Spacecraft', Acta Astronautica, 35, Suppl. 635-644, 1995

Prado, J.Y., Perret, A., Pignolet, G. & Dandouras, I., 'Using a Solar Sail for a Plasma Storm Early Warning System', IAA-96-IAA.3.3.06, 47th International Astronautical Congress, October 1996

Leipold, M., 'ODISSEE - A Proposal for Demonstration of a Solar Sail in Earth Orbit', IAA-L98-1005, 3rd International Academy of Astronautics Conference on Low Cost Planetary Missions, Pasadena, April 1998

McInnes, C.R., 'Mission Applications for High Performance Solar Sails', IAA-L.98-1006, 3rd IAA International Conference on Low-Cost Planetary Missions, Pasadena, April 1998

Gershman, R. & Seybold, C., 'Propulsion Trades for Space Science Missions', IAA-L.98-1001, 3rd IAA International Conference on Low-Cost Planetary Missions, Pasadena, April 1998

Carroll, K.A., 'Economical Planetary Space Science Using Small Solar Sail Propelled Spacecraft', Proceedings of the 10th Conference on Astronautics, CASI (Canadian Aeronautics and Space Institute), Ottawa, October 1998

Solar sailing books

Polyakhova, E., Space Flight Using a Solar Sail -The Problems and the Prospects, Kosmicheskiy Polet Solnechnym Parusom, Moscow, 1986, [in Russian]

Friedman, L., Star Sailing: Solar Sails and Interstellar Travel, Wiley Science Publications, New York, 1988

Clark, A.C., [ed.] Project Solar Sail, Penguin Group Books, New York, 1990

Wright, J.L., Space Sailing, Gordon and Breach Publishers, Philadelphia, 1992

Souza, D.M., Space Sailing, Lerner Publications Company, Minneapolis, 1994

McInnes, C.R.: Solar Sailing: Technology, Dynamics and Mission Applications, Springer-Verlag, ISBN 1-85233-102-X, 1999

Solar sail internet sites

http://www.ugcs.caltech.edu/~diedrich/solarsails/

http://www.ec-lille.fr/~u3p/index.html

http://www.kp.dlr.de/solarsail/

Appendix B: Artificial Lagrange points

B1. Introduction

This section will examine the artificial Lagrange point problem with a partially reflecting solar sail, since a real aluminised sail film will typically have a reflectivity of order 0.9. Firstly, equilibrium solutions will be obtained for an ideal solar sail. Then, the problem will be re-visited with a partially reflecting solar sail. Apart from reducing the magnitude of the radiation pressure force exerted on the solar sail, the finite absorption of the sail means that the radiation pressure force vector is no longer directed normal to the sail surface. Due to this effect, it will be shown that the volume of space available for artificial Lagrange points is extremely sensitive to the solar sail reflectivity.

B2. Equilibrium solutions for an ideal solar sail

Firstly, equilibrium solutions for an idealised, perfectly reflecting solar sail will be derived. The ideal sail will be considered in a frame of reference co-rotating with two primary masses m_1 (Sun) and m_2 (Earth or other planet) at constant angular velocity $\boldsymbol{\omega}$, as shown in Fig. B1. The sail attitude is defined by a unit vector **n** normal to the sail surface, fixed in the rotating frame of reference. In addition, the ratio of the solar radiation pressure force to the solar gravitational force exerted on the sail is defined by the sail lightness number β. Since both forces have an inverse square variation with solar distance the sail lightness number is a constant. It can be shown that the sail lightness number is related to the total solar sail mass per unit area by σ [g m^{-2}]=1.53/β. The units of the problem will be chosen such that the gravitational constant, the distance between the two primary masses and the sum of the primary masses are all taken to be unity.

The vector equation of motion for a solar sail in this rotating frame of reference may be written in standard form as

$$\frac{d^2\mathbf{r}}{dt^2} + 2\boldsymbol{\omega} \times \frac{d\mathbf{r}}{dt} + \nabla U = \mathbf{a} \qquad (1)$$

with the three-body gravitational potential U and the solar radiation pressure acceleration **a** defined by

$$U = -\left[\frac{1}{2}\left(x^2 + y^2\right) + \frac{1-\mu}{r_1} + \frac{\mu}{r_2}\right] \qquad (2a)$$

$$\mathbf{a} = \beta \frac{1-\mu}{r_1^2}\left(\hat{\mathbf{r}}_1.\mathbf{n}\right)^2 \mathbf{n} \qquad (2b)$$

where $\mu = m_2/(m_1 + m_2)$ is the mass ratio of the system and the sail position vectors are defined as $\mathbf{r}_1 = (x+\mu, y, z)$ and $\mathbf{r}_2 = (x-(1-\mu), y, z)$.

Equilibrium solutions are now required in the rotating frame of reference so that the first two terms of Eq. (1) vanish. The five classical Lagrange points are then obtained as the solutions to $\nabla U = 0$ with $\hat{\mathbf{r}}_1.\mathbf{n} = 0$ and so **a**=0. However, for $\hat{\mathbf{r}}_1.\mathbf{n} \succ 0$ there is an additional acceleration **a** which is a function of the lightness number β and attitude **n** so that new artificial equilibrium solutions may be generated. Since the vector **a** is oriented in direction **n**, taking the vector product of **n** with Eq. (1) it follows that

$$\nabla U \times \mathbf{n} = 0 \;\Rightarrow\; \mathbf{n} = \lambda \nabla U \tag{3}$$

where λ is an arbitrary scalar multiplier. Using the normalisation condition $|\mathbf{n}|=1$, λ is identified as $|\nabla U|^{-1}$ so that the required sail attitude is defined by

$$\mathbf{n} = \frac{\nabla U}{|\nabla U|} \tag{4}$$

which can be used to obtain the sail pitch angle α. The required sail lightness number may also be obtained by taking a scalar product of Eq. (1) with **n**. Again requiring an equilibrium solution it is found that

$$\beta = \frac{r_1^2}{(1-\mu)} \frac{\nabla U.\mathbf{n}}{(\hat{\mathbf{r}}_1.\mathbf{n})^2} \tag{5}$$

Since the sail lightness number and attitude can be selected, the set of five classical Lagrange points will be replaced by an infinite set of artificially generated equilibrium solutions.

The regions in which these new solutions may exist are defined by the constraint $\hat{\mathbf{r}}_1.\nabla U \geq 0$ with a boundary surface defined by an equality. This constraint may be understood physically since the solar radiation pressure acceleration vector **a**, and so the sail attitude vector **n**, can never be directed sunward. The boundary surface has two topologically disconnected surfaces S_1 and S_2 which define the region of existence of equilibrium solutions near the m_2, as shown in Fig. B2. The classical equilibrium solutions lie on either S_1 or S_2 since they are the solutions to $\nabla U = 0$. Surfaces of constant sail lightness number generated from Eq. (5) for the Earth-Sun system are also shown in Fig. B2. In general, the surfaces of constant sail lightness number approach these boundaries asymptotically with $\beta \to \infty$ when $\hat{\mathbf{r}}_1.\nabla U \to 0$ as is clear from Eq. (5). It can be seen that as the sail lightness number increases larger volumes of space are accessible for artificial equilibrium points.

B3. Equilibrium solutions for a partially reflecting solar sail

A realistic solar sail force model which includes absorption will now be considered. To allow a closed-form solution, the solar sail will be assumed to have perfect

specular reflectivity and no thermal re-emission but will still have an overall reflectivity η less than unity. Then, the radiation pressure acceleration will act in direction **m** and may be written as the sum of components normal **n** and transverse **t** to the sail surface

$$a\mathbf{m} = \frac{1}{2}\beta\frac{1-\mu}{r_1^2}(1+\eta)(\hat{\mathbf{r}}_1.\mathbf{n})^2\mathbf{n} + \frac{1}{2}\beta\frac{1-\mu}{r_1^2}(1-\eta)(\hat{\mathbf{r}}_1.\mathbf{n})(\hat{\mathbf{r}}_1.\mathbf{t})\mathbf{t} \qquad (6)$$

It can be seen that the main effect of the non-perfect reflectivity of the sail is to reduce the acceleration magnitude and to introduce an off-set in the direction of the radiation pressure acceleration. The acceleration now acts in direction **m** rather than normal to the sail surface in direction **n**. This off-set is defined by the centre-line angle ϕ with the actual radiation pressure force direction defined by the cone angle θ, as shown in Fig. B1.

The analysis presented in the previous section will be repeated using the sail force model defined by Eq. (6) so that the equation of motion may now be written as

$$\frac{d^2\mathbf{r}}{dt^2} + 2\boldsymbol{\omega}\times\frac{d\mathbf{r}}{dt} + \nabla U = a\mathbf{m} \qquad (7)$$

For an equilibrium solution the first two terms of Eq. (7) will again vanish so that the sail attitude must be chosen as

$$\mathbf{m} = \frac{\nabla U}{|\nabla U|} \qquad (8)$$

The unit vector **m** can now be defined by the cone angle θ between the radial direction $\hat{\mathbf{r}}_1$ and **m** as

$$\tan\theta = \frac{|\hat{\mathbf{r}}_1\times\nabla U|}{\hat{\mathbf{r}}_1.\nabla U} \qquad (9)$$

In addition, using Eq. (6) the centre-line angle can be obtained from the ratio of the transverse and normal accelerations as

$$\tan\phi = \frac{1-\eta}{1+\eta}\tan\alpha \qquad (10)$$

where the sail pitch angle $\alpha=\theta+\phi$. Noting that **n.t**=0 and taking a scalar product of Eq. (7) with the unit vector **n** gives the required sail lightness number as

$$\beta = \frac{2r_1^2}{1-\mu}\frac{\nabla U.\mathbf{n}}{(1+\eta)(\hat{\mathbf{r}}_1.\mathbf{n})^2} \tag{11}$$

The centre-line angle may be obtained explicitly by again noting that $\alpha=\theta+\phi$. Then, after some reduction, Eq. (10) yields the centre-line angle directly from the cone angle as

$$\tan\phi = \frac{\eta}{(1+\eta)\tan\theta}\left[1-\left[1-\frac{1-\eta^2}{\eta^2}\tan^2\theta\right]^{1/2}\right] \tag{12}$$

Lastly, using Eq. (11) it is found that the required sail lightness number may be obtained in terms of the lightness number for an ideal solar sail $\tilde{\beta}$ as

$$\beta = \frac{2}{(1+\eta)}\frac{\sqrt{1+\tan^2\phi}}{(1-\tan\theta\tan\phi)^2}\tilde{\beta} \tag{13}$$

where $\tilde{\beta}$ is defined by Eq. (5). Therefore, using Eqs. (9), (12) and (13) the sail orientation and sail lightness number required for an artificial equilibrium solution can be obtained.

The effect of a non-ideal solar sail is shown in Fig. A3 for a reflectivity of 0.9, typical of an aluminised sail film. Firstly, it can be seen that the volume of space available for equilibrium solutions about L_2 is significantly reduced. This is due to the centre-line angle which limits the direction in which the radiation pressure force vector can be oriented. For solutions near L_1 the main effect of the non-ideal sail is to displace the equilibrium solutions towards the Earth. This is due to the reduction in the magnitude of the radiation pressure force, rather than the centre-line angle. In general then, equilibrium solutions sunward of L_1 are not greatly effected by a realistic sail while equilibrium solutions about L_2 are severely restricted.

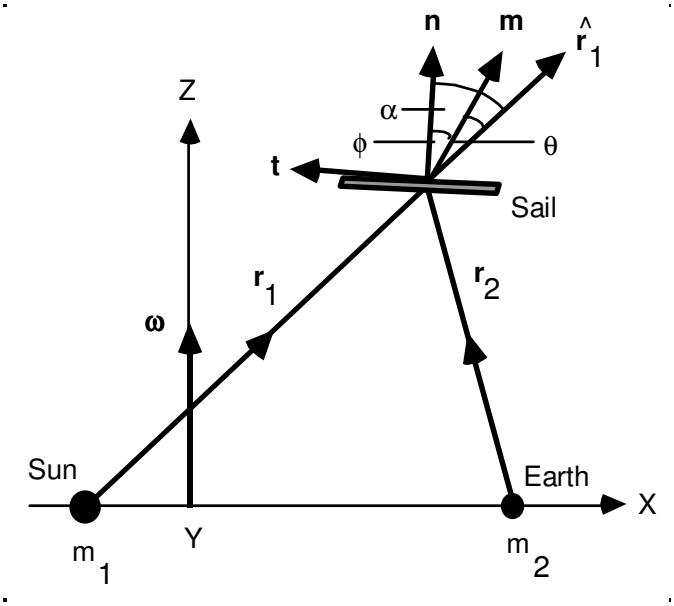

Figure B1. Sun-Earth restricted three-body problem with a partially reflecting solar sail.

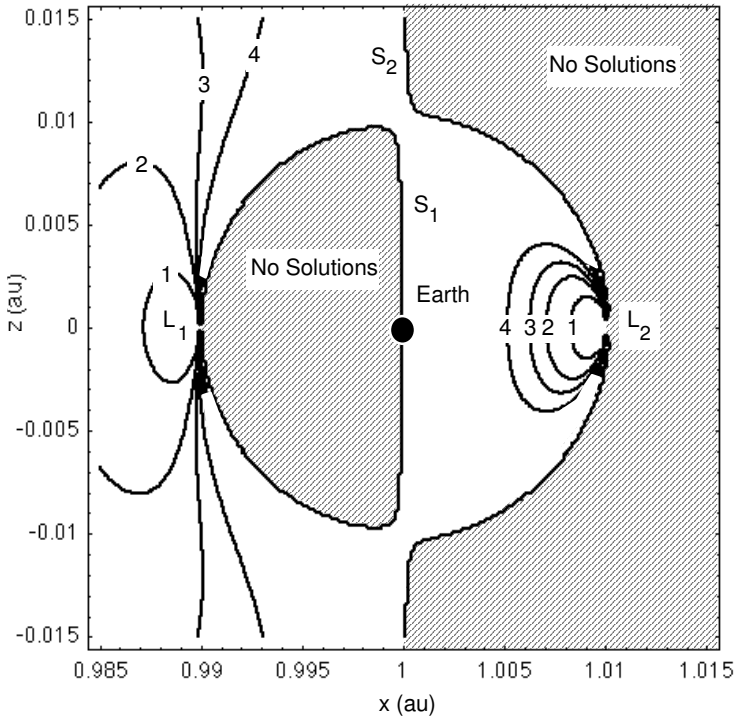

Figure B2. Contours of sail loading in the x-z plane with reflectivity η=1. Contours (gm^{-2}): [1] 76.5 [2] 38.25 [3] 25.5 [4] 15.3

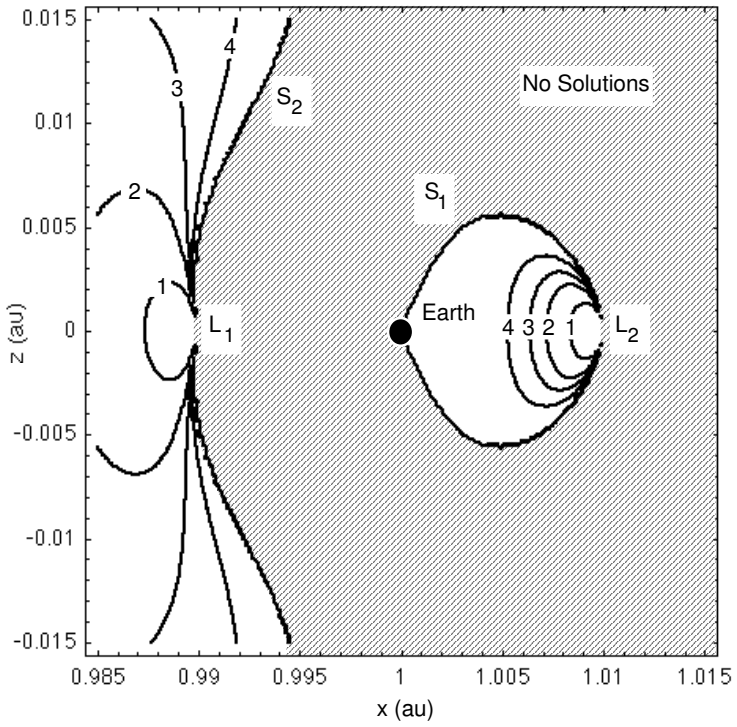

Figure B3. Contours of sail loading in the x-z plane with reflectivity η=0.9. Contours (gm^{-2}): [1] 76.5 [2] 38.25 [3] 25.5 [4] 15.3

Appendix C: NPOESS Polar Relay Satellite Requirements

C.1 Introduction

This white paper provides design considerations and results for a communication satellite for the purpose of data transfer from the NPOESS satellite constellation to NPOESS ground stations. The satellite under consideration is unique in that it is a stationary, polar located satellite, using a non-keplerian orbit with attitude and position controlled by solar sails. The satellite under design was dubbed NPRS (NPOESS Polar Relay Satellite).

C.2 Conclusion

The NPRS design trade space included four design cases. The design trade-off included orbit locations of 9E5 (900,000) Km and 3.9E6 (3,900,000) Km, and data rates of 20 Mbps and 40 Mbps. The result of the trade shows that the additional EIRP required to close the link between the NPOES and NPRS satellites will results in a large impact to the NPOESS design. Increasing the NPRS aperture to make up the required EIRP will result in an aperture so large that two antennas and pointing would be required on the NPRS satellite. The design case that appears to offer the most promising NPRS spacecraft communication payload is the 900,000 Km case, however, the 27 to 30 dB of additional EIRP from NPOESS needed to realize this design, while maintaining a single aperture, may be impractical.

C.3 Design Methodology

Currently NPOESS is in Source Selection and NPOESS payload parameters are undefined. Information for this paper was obtained from the NPOESS TRD dated 23 January, 2002 and does not represent source selection sensitive material. The NPRS design was to effectively duplicate TDRSS service to NPOESS. TDRSS services to NPOESS provide a method of delivering data to the ground when NPOESS satellites are not in view of the CDA (NPOESS ground site).

The design of NPRS was performed while adhering to the following design considerations:

- As much as possible, maintain the current design of NPOESS communication subsystem.
- NPOESS is assumed to have a continual line of site to NPRS while in the polar regions.
- Since NPRS attitude and position control is to be maintained by solar sails, minimize the antenna size on NPRS.
- Required data rate through NPRS is 20 Mbps or 40 Mbps.
- Required altitude of NPRS is 9E5 Km or 3.9E6 Km.

C.4 NPOESS Background Data

Tables C.1- C.4 provide information regarding the NPOESS Ground Station and TDRSS services.

Table C.1 Ground Station Element - SMD Downlink Parameters

	Parameter:	**NPOESSS Value:**
	Data Rate:	400 Mbps Max (TBR)
	Modulation:	SQPSK (TBR)
	Coding:	(255,223) Reed Solomon with I=4 (TBR)
	Convolutional Encoding: Code Rate Constraint Length Connection Vectors Phase relationship Symbol inversion Puncturing	 ½ (TBR) 7 bits (TBR) G1=1111001/G2=1011011 (TBR) G1 assoc with first symbol (TBR) TBD No
	Randomization	(Same as HRD)
	Maximum Occupied Bandwidth:	375 MHz
	E_b/N_o:	TBD
	BER after decoding	$< 10^{-8}$
	Frequency:	8212.5 MHz
	Polarization	Selectable Left/Right Hand Circular (TBR)
	Ground Aperture Size:	13 meters (TBR)
	Ground G/T:	33.1 dB/K (TBR)
	Data Format:	TBD
	Frequency:	26250.0 MHz
	Maximum Occupied Bandwidth:	400 MHz (TBR)
	Polarization	Selectable Left/Right Hand Circular (TBR)
	Satellite Aperture Size:	TBD
	Satellite EIRP:	TBD
	Ground Aperture Size:	TBD
	Ground G/T:	TBD
	Data Format:	TBD

Table C.2 Space Network Forward Link Parameters

Link:	Parameter:	NPOESSS Value:
a. LEO&A Only	Modulation:	UQPSK
	Coding:	BCH
	Convolutional Encoding: Code Rate Constraint Length Connection Vectors Phase relationship Symbol inversion Puncturing	 ½ (TBR) 7 bits (TBR) G1=1111001/G2=1011011 (TBR) G1assoc with first symbol (TBR) TBD No
	Randomization	TBD (Same as HRD)
	BER	$<10^{-5}$ Physical BER
	Polarization	Right Hand Circular
Command Crosslink:	Data Rate:	125 bps, 1.0 kbps (TBR)
	Maximum Occupied Bandwidth:	2 kHz (TBR)
	E_b/N_o:	TBD
TDRSS SA @ S-Band:	Frequency (USB):	2106.4 MHz
	Satellite Aperture Size:	TBD
	TDRSS EIRP:	TBD
	Satellite G/T:	TBD
b. TDRSS SA @ K_u-Band:		
Calibration Table Upload Crosslink:	Data Rate:	256 kbps (TBR)
"Routine Commanding"	Occupied Bandwidth:	TBD
	E_b/N_o:	TBD
	Frequency:	13775 MHz
	Polarization	TBD
	TDRSS EIRP:	TBD
	Satellite G/T:	TBD

Table C.3 Space Network K_u-Band Return Link

Link:	Parameter:	NPOESSS Value:
TDRSS SA K_u-Band: SMD	Data Rate:	150 Mbps (TBR)
	Modulation:	SQPSK
	Coding:	(255, 223) Reed Solomon with I=4 (TBR)
	Convolutional Encoding: Code Rate Constraint Length Connection Vectors Phase relationship Symbol inversion Puncturing	 TBD TBD G1=TBD/G2=TBD TBD TBD TBD
	Randomization	TBD
	Maximum Occupied Bandwidth:	TBD
	E_b/N_o:	TBD
	BER	$< 10^{-5}$ Physical BER
	Frequency:	15003.4 MHz
	Satellite Aperture Size:	TBD
	Satellite EIRP:	TBD
	TDRSS Received Power:	TBD
	Polarization	Selectable Left/Right Hand Circular

Table C.4 Space Network S-Band Return link

Link:	Parameter:	NPOESSS Value
TDRSS SA Telemetry Crosslink:	Data Rate:	2 kbps; 16 kbps (TBR)
	Modulation:	SQPN
	Coding:	(255, 223) Reed Solomon with I=4 (TBR)
	Convolutional Encoding: Code Rate Constraint Length Connection Vectors Phase relationship Symbol inversion Puncturing	 ½ (TBR) 7 bits (TBR) G1=1111001/G2=1011011 (TBR) G1assoc with first symbol (TBR) TBD No
	Randomization	TBD
	Maximum Occupied Bandwidth:	TBD
	E_b/N_o:	TBD
	BER	$< 10^{-5}$ Physical BER
	Frequency (USB):	2287.5 MHz
	Satellite Aperture Size	TBD
	Satellite EIRP:	TBD
	TDRSS Received Power:	TBD
	Polarization	Right Hand Circular

C.5 NPOESS Communication Subsystem Changes

From the above tables it was observed that NPOESS has both S-Band and Ku-Band Single Access, Forward and Return TDRSS services. The design trade space for NPRS requires data transfer at 20 Mbps or 40 Mbps. Since only Ku-Band Single Access provides service at this high of a data rate, the S-Band TDRSS service is removed from NPOESS and the Ku-Band TDRSS service for NPOESS is assumed changed to provide a compatible modulation format with the 25.250 GHz downlink. Also, since the design trade space is primarily concerned with downlink, or Return data services; the current NPOESS has a Forward data service at 256 Kbps, which is also removed and not supported by NPRS.

Although the NPOESS Communication Subsystem is undefined, we assume that the configuration that will be put into place will provide sufficient EIRP to close the communication links to the geosynchronous orbiting TDRSS satellite. The following information is from the NPOESS TRD:

- NPOESS orbit is 833 km
- NPOESS Ku-Band Return Single Access Frequency is 15.0034 GHz
- Data rate between NPOESS and TDRSS is 150 Mbps
- Given these parameters, the NPOESS to TDRSS EIRP requirement is approximately 52 dB. Conceptually, this can be achieved using a 4-foot diameter parabolic reflector at 55% efficiency with a 20 - Watt transponder.

Table C.5 shows the result of changes to the NPOESS EIRP requirement due to NPRS Return data rate or altitude changes.

Table C.5 Case Study Requirements and EIRP Resultant EIRP Change

Case Study Requirement	EIRP Delta
3.9 million Km	40.84 dB
0.9 million Km	28.1 DB
20 Mbps	-8.75 dB
40 Mbps	-5.74 dB

Table C.6 provides permutations of the Case Study Requirements that result in the four Case Studies, and the overall change in EIRP that is needed to close the link between NPOES and NPRS.

Table C.6 Case Studies and EIRP Requirements

Case Study	EIRP Delta
3.9 million Km/20 Mbps	32.09
3.9 million Km/40 Mbps	35.1
0.9 million Km/20 Mbps	19.35
00.9 million Km/40 Mbps	22.36

From the above information the design architect realizes the design for NPOESS and NPRS converges when this additional EIRP is realized. The additional EIRP can be realized by changing data rate, antenna size, frequency, or transmitter output power.

Two things are immediately observable given this little information:

- The additional EIRP requirement is large
- A large antenna design will be limited at the point that the antenna aperture is so large (the FOV is so small) that the antenna footprint does not extend over the NPOESS orbit. At this point, two antenna would be required, one for the transfer orbit link and the other for the space to ground link. Additionally, the transfer orbit link would require gimbals.

The following tables lists NPRS communication payload requirements for the various design cases, and assumes an NPOESS communication subsystem design using 15.0034 GHz, a 4-foot dish, and 20 Watts, providing 52 dB of EIRP.

For the 3.9 million km design case, and the 0.9 million Km case, the NPRS antenna size is defined as the largest possible aperture that still provides the necessary footprint. This is the point that the design of the space architecture is considered to converge or be optimal as was commented on above. Table C.7 provides the additional EIRP for all design cases.

Table C.7 Case Studies and Resultant NPRS Antenna Size and Additional EIRP Requirements

Design Case **Altitude, Data Rate, Frequency** NPOESS Changes Removed S Band Forward Service Removed S Band Return Service Removed Ku Band Forward Service **Increase Ku Band Return Service EIRP by:**	**NPRS Antenna Size (feet)**	**Additional EIRP Required for Link Closure**
900,000 Km, 40 Mbps, 15.0034 GHz	4.4	30 dB
900,000 Km, 20 Mbps, 15.0034 GHz	4.4	27 dB
900,000 Km, 40 Mbps, 60 GHz	1.12	30 dB
900,000 Km, 20 Mbps, 60 GHz	1.12	27 dB
3.9 million Km, 40 Mbps, 15.0034 GHz	19.125	30 dB
3.9 million Km, 20 Mbps, 15.0034 GHz	19.125	27 dB
3.9 million Km, 40 Mbps, 60 GHz	4.78	30 dB
3.9 million Km, 20 Mbps, 60 GHz	4.78	27 dB

From the above table is observed for both 15.0034 GHz and 60 GHz cross-link frequencies, an additional 30 dB and 27 dB of additional EIRP will be required of NPOESS for the 40 Mbps and 20 Mbps cases, respectively.

This can only be accomplished by:

- Lowering the data rate to 40 Kbps.
- Increasing the NPOESS antenna size to 90 feet for the 15.0034 GHz and 20 Mbps case, or 85 feet for the 60 GHz and 20 Mbps case.
- Increasing the NPOESS output power to 9000 Watts (for the 20 Mbps case).
- A combination of the above.

Because of the TDRSS services that were removed from NPOESS, some weight and power should be able to be re-budgeted and used for these design cases, however; regardless of how the NPOESS satellite is changed, the necessary change can be said to be a very major impact to the NPOESS satellite.

C.6 NPRS Communication Payload Design

The design cases for the NPRS satellite consists of 4 design cases that represent each permutation of orbit/data rate pairs. Since the NPRS will relay data from the source directly to the ground, a design decision was made to bent-pipe the data through NPRS as opposed to creating a demodulation and re-modulation chain. This should result in significant weight and power savings.

A 13-meter ground aperture, as provided in Table C.1, was assumed for space to ground link services.

From Table C.7 the larger altitude of 3.9 million mm offer nothing additional to the design and will incur weight and power requirements above that of the 900,000 km orbit due to increased antenna size and larger output requirements for the downlink.

Both the 15.0034 GHz and 60 GHz cross-link frequencies result in antenna sizes that offer 70 % of earth coverage, which is assumed to include coverage of the ground stations. The design trade space for the NPRS satellite then becomes antenna size versus downlink power requirements.

Table C.8 NPRS Antenna Sizing and Output Power Requirements

Design Case **Altitude, Data Rate, Frequency**	**NPRS Antenna Size (feet)**	**Downlink Output Power at 25.250 GHz**
NPOESS Changes Removed S Band Forward Service Removed S Band Return Service Removed Ku Band Forward Service **Increase Ku Band Return Service EIRP by:**		
900,000 Km, 40 Mbps, 15.0034 GHz	4.4	40 Watts
900,000 Km, 20 Mbps, 15.0034 GHz	4.4	20 Watts
900,000 Km, 40 Mbps, 60 GHz	1.12	700 Watts
900,000 Km, 20 Mbps, 60 GHz	1.12	350 Watts

The 350 Watt and 700 Watt downlink power requirements for the 60 GHz case eliminates this as a design when compared to the 15.0034 GHz case. Although the aperture is larger for the 15.0034 GHz case, the design is much more reasonable than what would be required to realize 60 GHz at either 350 Watts or 700 Watts.

A weight and power budget for the 900,000 km, 15.0034 GHz, 20 Mbps and 40 Mbps data rates are provided in Table 9. A block diagram of the NPRS Communication Subsystem is shown in Figure C.1.

Figure C.1 NPRS Communication Payload Design

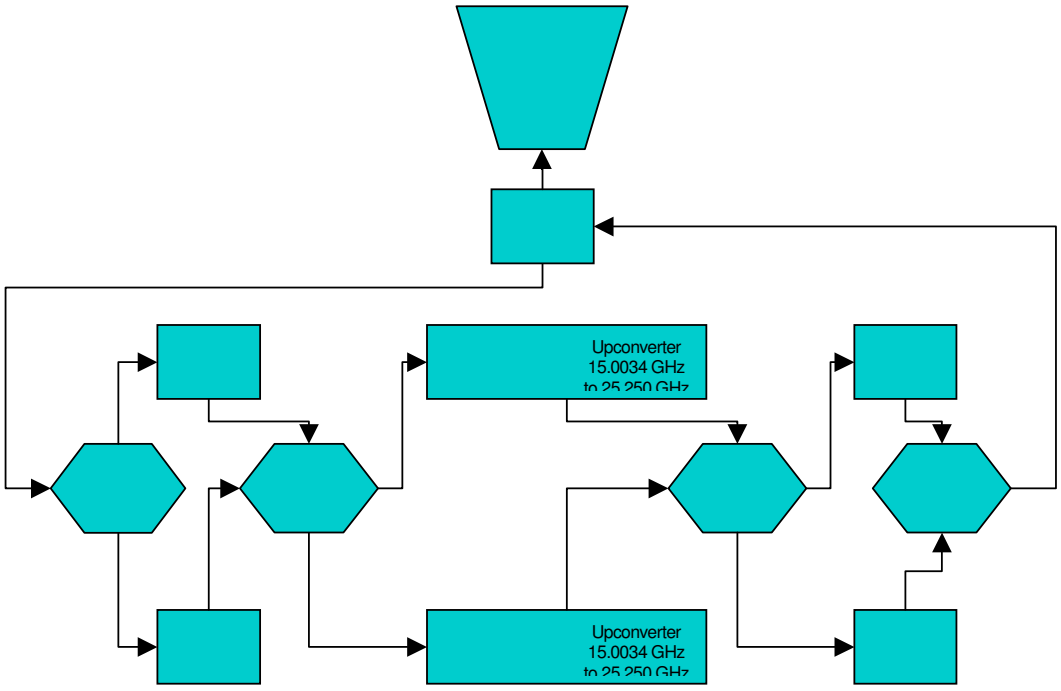

Table C.7 – Mass and Power Budgets

20 Mbps

Component	Prime	Redundant	Mass-Lbs	Power-DC W
UP/Down Link and Cross-Link Antenna	1			
LNA	1	1		
Amplifier – 20 Watts	1	1		
Upconverter	1	1		
Diplexer	1	1		
Local Osc	1	1		
Misc	4			
Total			**102**	**67**

40 Mbps

Component	Prime	Redundant	Mass-Lbs	Power-DC W
UP/Down Link and Cross-Link Antenna	1			
LNA	1	1		
Amplifier – 40 Watts	1	1		
Upconverter	1	1		
Diplexer	1	1		
Local Osc	1	1		
Misc	4			
Total			**110**	**112**

Appendix D: Alternative Analysis of NPOESS Polar Relay

D.1 Downlink Calculation

Downlink margin calculations from NPRS (NPOESS Polar Relay Satellite) are outlined below for NPRS altitudes of 900,000 km and 625,000 km. The round-trip light times (Earth to satellite and back) for these locations are 6 seconds and 4.2 seconds respectively.

Tracking coverage capability can be inferred from the minimum elevation angle of NPRS above the local horizon in the outlines below. Lowest elevations for Point Barrow occur in the summer, winter elevation angles are ~40 degrees higher.

Pt. Barrow (71.3N, 157W)

NPRS altitude 900,000 km

We take the following parameters from Appendix C:

antenna diameter = 1.2 m
transmitter power = 20 w
downlink carrier frequency = 25 Ghz (Ku)
transmission rate = 40 Mbps
bit error rate = 10^{-5}
Pt. Barrow ground station antenna diameter = 13 m

SSP (latitude of point directly beneath NPRS)
= 40 deg (summer solstice)
= 86 deg (winter solstice)

minimum elevation of NPRS above Pt. Barrow horizon (except for brief intervals)
= 20 deg (summer solstice, noon)

Assumptions for this analysis:

antenna efficiencies = 0.55 (ground and NPRS)
coding gain = 7 dB (BPSK Reed-Solomon, Viterbi, R-1/2)
antenna pointing error (maximum) = 20% beam width
antenna noise temperature = 700K
RF and media losses ~2.5 dB

Result:

Link margin = 6 dB. This is a satisfactory link closure. But heavy precipitation can degrade the link margin, leading to possible data losses.

Pt. Barrow (71.3N, 157W)

NPRS altitude 625,000 km

Assumptions for this analysis remain the same except for location.

Geometry:

SSP (latitude of point directly beneath NPRS)
= 21 deg (summer solstice)
= 68 deg (winter solstice)

minimum elevation of NPRS above Pt. Barrow horizon (except for brief intervals)
= 1.5 deg from northern horizon (*i.e.* over Arctic Ocean) (summer solstice, noon)

Result:

Link margin = 9 dB. This is a satisfactory link closure for the 40 Mbps rate and provides margin for precipitation and low elevation signal attenuation (~6 dB). The low elevation angle around the summer solstice is similar to the daily coverage now experienced year-round with GOES-3 at the South Pole station.

McMurdo Sound (78.3S, 165E)

NPRS altitude 625,000 km

Geometry:

SSP (latitude of point directly beneath the southern hemisphere NPRS)
= 21 deg (summer solstice)
= 68 deg (winter solstice)

minimum elevation of NPRS above McMurdo horizon (summer solstice, noon)
= 8 deg from southern horizon (*i.e.* over Transantarctic Mountains) (8 deg is adequate clearance)

Result:

Link margin = 9 dB. This closes the link for 40 Mbps and provides margin for precipitation.

Amundsen-Scott South Pole Station (90.0S, 0E)

NPRS altitude = 625,000 km

Geomety:

SSP (latitude of point directly beneath the southern hemisphere NPRS)
= 21 deg (summer solstice)
= 68 deg (winter solstice)

minimum elevation of NPRS above South Pole (summer solstice, noon)
= 20 deg from horizon

Result:

Link margin = 9 dB. Provides link closure and margin.

D.2 Crosslink Calculation Between NPOESS & NPRS

NPRS altitude = 625,000 km

We take the following parameters from Appendix C:

NPRS & NPOESS antenna diameters = 1.2 m
NPOESS transmitter power = 20 w
NPOESS altitude = 833 km
crosslink carrier frequency = 60 Ghz (V)
transmission rate = 40 Mbps
bit error rate = 10^{-5}

Assumptions for this analysis:

antenna efficiency = 0.55
coding gain = 7 dB (BPSK Reed-Solomon, Viterbi, R-1/2)
antenna pointing error (maximum) = 0.1 degree beam width *
antenna noise temperature = ~680 K *
RF losses = 2.0 dB *

Result:

Link margin = -5.6 dB. The additional EIRP required for link closure is about 6 - 7 dB, say 7 dB.

Comments:

The NPRS beam width footprint for this aperture/frequency does not cover the NPOESS orbit (and so coverage does not include ground stations).

* assumed performance parameters for crosslink design which differ from the downlink design

Some link closure options (for 60GHz crosslink):

1. Increase NPOESS transmitter power to 40 W, plus program-driven efficiency improvements to the antennas (e.g. phased array), RF, and on-board electronic systems to make up the deficit (~4 dB).

2. Increase NPOESS transmitter power to 40 W & NPOESS transmitting antenna diameter to ~2 m.

3. Maintain the current design and accept a transmission rate of 10 Mbps.

(Other options are possible that we have not addressed. For instance, an optical communication crosslink.)